Adsorption of Humic Acid from Water Using Metal-Organic Frameworks (MOFs): An Effective Removal Strategy

ABSTRACT:

The escalating presence of humic acid (HA) in aquatic systems poses significant ecological and potable water treatment challenges, altering the color, taste, and odor of water and fueling algal blooms that deplete oxygen levels to the detriment of aquatic life.

Traditional techniques like coagulation-flocculation, membrane filtration, oxidation fall short in efficiency due to its small fraction of HA, Humic acids (HAs) can interact with various organic and inorganic substances, affecting their characteristics and behavior in water. These interactions can influence the efficiency of water treatment processes like adsorption and coagulation. Specifically, HAs may compete with other contaminants for treatment sites or alter the chemical conditions of the treatment processes, impacting their effectiveness.

This thesis confronts the pervasive issue of HA contamination by leveraging the advanced properties of metal-organic frameworks (MOFs). In this work, four representative MOFs are synthesized and well characterized.

Then, their capability to enhance coagulation processes in water for HA and HA-kaolin treatment are detailed evaluated. The findings from this research extend beyond academic curiosity, offering actionable insights for water treatment facilities and environmental management agencies.

The synthesis of MOFs which are UiO-66(Zr), MIL-100(Fe), ZIF-8, and Al-fum. Each MOFs have been applied to remove HA by adsorption under different condition, effect of contact time, effect of initial pH, effect of adsorbent dosage. After adsorption experiment, MOF samples prepared to dry and went through characterization.

Removal of HA by MOF adsorption showed UiO-66(Zr) and MIL-100(Fe) examined shortest reaching equilibrium state with 10-15 min, however, ZIF-8 and Al-fum gradually reached equilibrium state after 60 min. Among various pH conditions, UiO-66(Zr) and MIL-100(Fe) showed the highest adsorption capacity under acidic conditions, while ZIF-8 excelled at neutral pH, and Al-fum exhibited the highest adsorption capacity under both acidic and basic conditions.

ZIF-8 has the highest adsorption capacity among the MOFs with capacity of 754 mg/g. MOF after adsorption samples went through characterizations and their remained characteristics indicating the adsorption not affected the structure of the MOFs.

Keywords: [Humic acid, MOFs Adsorption, UiO-66(Zr), MIL-100(Fe), ZIF-8, Al-fum}

1 Introduction

It has recently been found that the amount of natural organic matter (NOM) in water bodies varies and grows significantly [1]. The constituents of NOM can be categorized into two primary groups: complex heterogeneous humic compounds and non-humic substances, which comprise substances such as polysaccharides, hydrocarbons, carbohydrates, lipids, waxes, resins, and low molecular organic acids [1]. These substances give water its color and aid in the transmission of micropollutants[33,34]. Their presence also has an adverse effect on the water's flavor and smell. It is estimated that half of the organic carbon in water is composed of humic molecules [2, 3]. All organic materials present in natural water systems are referred to as Natural Organic Matter (NOM), of which Dissolved Organic Matter (DOM) is a subset. When water passes through a filter that can capture particles larger than a few tenths of a micron, the portions of NOM that are small enough to stay in solution are referred to as DOM. One important part of decomposed organic matter (DOM) is humic acid (HA), which is made up of a number of complex compounds that are produced by the chemical and biological degradation of plant and animal matter. These molecules can greatly affect the chemical and biological characteristics of water due to their capacity to form soluble complexes with ions and their yellow to dark brown color. Water can have its chemical and physical properties changed by humic acid.

The study aims to optimize the operating conditions for a hybrid process combining Metal-Organic Frameworks (MOFs) with coagulation to enhance the removal of dissolved organic matter (DOM) from wastewater. The specific objectives include Identifying suitable synthesis methods and preparations for various MOFs with optimal characteristics, and investigating the optimal parameters for MOF adsorption Materials and methods the most and determining the most efficient MOF for humic acid (HA) removal.

The research will contribute to developing advanced technologies for DOM removal, protecting the environment and human health. It will provide valuable insights for optimizing and designing wastewater treatment plants and inform policymakers on sustainable wastewater treatment strategies. The significance of this study lies in its potential to develop an effective and sustainable method for removing humic acid (HA) from tap water[4]. This is crucial due to the environmental and health issues caused by HA in tap water. Utilizing Metal-Organic Frameworks (MOFs) in water treatment is a novel approach, offering a promising solution to wastewater treatment challenges[5]. By investigating the efficacy of MOFs in HA removal, this study aims to contribute to the advancement of new wastewater treatment technologies and provide insights into using MOFs to overcome the limitations of traditional coagulation processes. Additionally, the study will focus on optimizing process parameters and conducting an economic feasibility analysis. We examined four different types of MOFs: Zirconium 1,4-dicarboxybenzene (UiO-66(Zr)), Matériaux de l'Institut Lavoisier with iron (MIL-100(Fe)), zeolitic imidazolate framework-8 (ZIF-8), and Aluminum-fumarate based MOF (Al-fum). Our findings will identify the most effective MOF for adsorption and removal efficiency.

From previous studies, it is evident that adsorption, separation processing, coagulation-flocculation, precipitation, and oxidation are the most common technologies used for wastewater treatment[6]. Some of these processes are inefficient, have operating issues, demand a substantial amount of energy, and are not economically favorable when compared to adsorption approaches. Therefore, the usage of nano-based materials to address these flaws and improve the efficiency of these processes has recently expanded. Nanoparticles such as titanium dioxide (TiO2), carbon nanotubes (CNTs), silver (Ag), zinc oxide (ZnO), activated carbon, and graphene have demonstrated cost-effectiveness and efficiency benefits. A new class of porous materials was developed to deal with this intricate production of nanoparticles. Metal-organic frameworks (MOFs) are a novel type of porous crystalline solids made up of single metal ions or clusters coordinated by organic linkers with a strong connection[7]. MOFs feature a large surface area, a variable pore size, and the ability to be

adjusted to target certain contaminants. MOFs have attracted interest as a promising adsorbent for wastewater treatment due to their unique features. MOFs have demonstrated outstanding effectiveness in wastewater treatment in recent years, owing to their flexible structure. Notably, water stability is a significant consideration for MOF wastewater treatment applications[8]. Thus, water-stable MOFs are often created for wastewater treatment operations because they can keep their structure in water. The initial breakthrough in MOFs for wastewater treatment was made in 1997 by Yaghi et al. [9], when it was discovered that the performance of zeolites and activated carbon (AC) was deteriorating owing to structural faults; hence, the demand for water-stable materials became a need [10].MOFs have been examined for their ability to remove a variety of contaminants, including heavy metals, organic chemicals, and colors[11]. Because of the tunable property of MOFs, several MOF-templated materials, including virgin MOFs, modified MOFs, and magnetic MOFs composites, have been created and employed for eliminating divalent heavy metal ions.

UiO-66(Zr) is highly effective for adsorbing humic acid (HA) and improving coagulation in water treatment due to its high adsorption capacity and mesoporous structure. Jiang et al. found it has a very high maximum adsorption capacity for HA, following the Langmuir model [12]. Lin and Chang's research showed that surfactants could enhance NH2-UiO-66, a variant of UiO-66(Zr), resulting in a maximum adsorption capacity of 108.93 mg/g and 95.0% removal effectiveness [13]. HA adsorption on UiO-66(Zr) involves hydrogen bonding, π-π interactions, and electrostatic interactions, contributing to its high affinity for HA. Jiang et al. found the adsorption process to be spontaneous and endothermic [12]. UiO-66(Zr) is stable in various aqueous conditions, maintaining its efficacy over time. Lin and Chang confirmed its stability under different pH levels and temperatures[14]. UiO-66(Zr) improves coagulation processes. Jiang et al. reported that Zr-MOFs with surface modifications enhance interactions with HA, aiding flocculation and coagulation [12, 13]. Lin and Chang suggested NH2-UiO-66's mesoporous structure offers more nucleation sites for floc formation [12]. UiO-66(Zr) maintains high adsorption efficiency even with competing ions and organic materials. Lin and Chang showed stability in solutions with varying NaCl concentrations [20]. UiO-66(Zr) is cost-effective and environmentally friendly, as it can be recycled and reused for HA adsorption. Lin and Chang demonstrated that NH2-UiO-66 could be restored with a simple ethanol wash and reused while maintaining high removal effectiveness[13].

MIL-100(Fe) effectively removes humic acid (HA) from water due to its high adsorption capacity, large surface area, and abundance of active sites. Nehra et al. reported a maximum phosphate adsorption capacity of 93.6 mg/g for MIL-100(Fe), suggesting high adsorption effectiveness for HA and other contaminants [15]. MIL-100(Fe) is known for its excellent structural stability in aquatic conditions, crucial for sustained adsorption efficacy. Studies on CoFe2O4@MIL-100(Fe) hybrid magnetic nanoparticles demonstrated rapid uptake rates and high adsorption capacities for arsenic, highlighting the mesoporous nature's role in fast adsorption and high capacity [16]. HA adsorption on MIL-100(Fe) involves hydrogen bonding, π-π interactions, and electrostatic interactions, contributing to a significant affinity between HA and the framework. Xu et al.'s work on antimony and arsenic elimination emphasized the importance of complexation and electrostatic interactions in the adsorption process [16]. MIL-100(Fe) has proven effective in real-world water treatment, with Nehra et al.'s studies using actual water samples showing successful phosphate removal, indicating potential for broader water management applications [15]. The superior anti-interference capacity of MIL-100(Fe) ensures high adsorption efficiency even with competing ions and organic materials, as demonstrated in research on CoFe2O4@MIL-100(Fe) hybrid nanoparticles[16].

The study by Lin and Chang demonstrated that ZIF-8 has a surprisingly high adsorption capacity for humic acid, surpassing other adsorbents like activated carbon, fly ash, zeolites, and graphite, making it an ideal candidate for HA removal and coagulation enhancement in water treatment [17]. ZIF-8's remarkable adsorption capacity is attributed to π-π stacking interactions between its imidazole groups and the benzene rings of humic acid, as well as

electrostatic interactions between ZIF-8's positive surface and the acidic sites of HA. These interactions explain ZIF-8's strong affinity for humic acid. Lin and Chang noted that humic acid adsorption onto ZIF-8 is enhanced in acidic conditions, beneficial for water treatment scenarios where pH adjustment can improve HA removal efficiency [18]. Additionally, ZIF-8 maintains stable humic acid adsorption across a wide range of NaCl concentration solutions, making it effective for water sources with varying salinity levels. ZIF-8 is also cost-effective and environmentally friendly, as it can be easily recycled by ethanol washing and reused for HA adsorption. Although the study does not specifically mention coagulation improvement, ZIF-8's positive surface charge suggests potential interactions with flocculants or other negatively charged coagulants, potentially enhancing the coagulation process for HA removal [19].

The article "Fumarate-based metal-organic frameworks as a new platform for selective removal of fluoride from brick tea infusion"[20] explores the use of aluminum fumarate (Al-fum) for removing humic acid (HA) from water and improving coagulation, particularly in the presence of HA and HA-kaolin. Although the study primarily focuses on fluoride removal, it highlights the potential of fumarate-based MOFs like Al-fum for pollutant removal, including HA. The study demonstrates the excellent adsorption capacity of MOF-801, which removed over 80% of fluoride in 5 minutes at ambient temperature[20]. This suggests that fumarate-based MOFs have active sites that interact with various pollutants, including HA, which can form compounds with these functional groups [21]. The large surface area and functional groups of fumarate-based MOFs can enhance coagulation processes by providing more nucleation sites for floc formation, crucial for reducing turbidity in the presence of HA and HA-kaolin [20]. HA adsorption onto Al-fum occurs through mechanisms similar to fluoride adsorption, involving complexation with functional groups on the MOF surface and electrostatic interactions. Al-fum improves coagulation in water treatment procedures by providing additional locations for floc production. This addition helps reduce turbidity and remove humic acid, particularly in situations when HA-kaolin conditions are present.

2 Materials and methods

In our experiment, humic acid was first simulated under laboratory conditions. Subsequently, four different types of Metal-Organic Frameworks (MOFs) were synthesized: UiO-66(Zr), MIL-100(Fe), ZIF-8, and Al-fum. These MOFs underwent characterization using X-ray Diffraction (XRD) for assessing crystallinity, Brunauer-Emmett-Teller (BET) analysis for determining surface area properties, nitrogen adsorption for defining micro or mesoporous nature, Fourier-Transform Infrared Spectroscopy (FTIR) for identifying functional groups, and Scanning Electron Microscopy (SEM) for examining morphology and shape. Each MOF was then tested for its ability to remove humic acid under different conditions, including kinetic adsorption to study the effect of time, pH to determine the optimal pH for removal, and isotherm adsorption to evaluate the effect of MOF dosage. After completing the isotherm adsorption tests, the MOF solutions were dried through centrifugation and vacuum drying. The dried MOFs were characterized again using XRD, SEM, and FTIR to investigate the effects of adsorption on the MOF structure and functionality of the MOF groups.

2.1 Chemicals

All the chemical used with manufacturer name and more details have been provided fromTable 1.

Table 1. Chemical used in the experiments

Reagent	Molecular Formula	Grade	Reagent Manufacturer
Humic acid	$C_9H_9NO_6$	AR	Shanghai Aladdin Biochemical

			Technology Co., Ltd
Sodium Hydroxide	NaOH	AR	Sinopharm Chemical Reagent Co., Ltd.
Hydrochloric Acid	(HCl)	AR	Sinopharm Chemical Reagent Co., Ltd.
N, N-Dimethyl-formamide (DMF)	$HCON(CH_3)_2$	AR	Sinopharm Chemical Reagent Co., Ltd.
Zirconium dichloride oxide octahydrate	$Cl_2H_{18}O_9Zr$	AR	J&K Scientific Ltd
Terephthalic acid	$C_8H_6O_4$	AR	TCI
Formic acid	HCOOH	AR	Sinopharm Chemical Reagent Co., Ltd.
Methanol anhydrous	CH_3OH	AR	Sinopharm Chemical Reagent Co., Ltd.
Ethanol absolute	C_2H_6O	AR	Sinopharm Chemical Reagent Co., Ltd.
Iron (III) chloride hexahydrate for synthesis	$FeCl_3{\cdot}6H_2O$	AR	J&K Scientific Ltd
1,3,5-benzenetricarboxylic acid trimesic acid (H_3BTC)	$C_9H_6O_6$	AR	TCI
zinc acetate dihydrate Zn $(OAc)_2$	$Zn(C_2H_3O_2)_2{\cdot}2H_2O$	AR	Shanghai Aladdin Biochemical Technology Co., Ltd
2-Methylimidazole (Hmim)	$C_4H_6N_2$	AR	Shanghai Aladdin Biochemical Technology Co., Ltd
Aluminum chloride hexahydrate	$AlCl_3{\cdot}6H_2O$	AR	Sigma-Aldrich Chemical Company
Fumaric acid	$C_4H_4O_4$	AR	TCI
Poly-aluminum chloride (PAC)	$[Al_2(OH)nCl_6\text{-}n]m$	AR	Shandong Jiahua water treatment technology Co., Ltd

2.2 Instruments

All instruments that used in the experiments with their model name and manufacturer have been listed inTable 2.

Table 2. Instruments used in the experiments

Instrument name	Model	Manufacturer
Electronic Analytical Balance	BSA124S-CW	Sartorius, Germany
Vacuum Drying Oven	DZF-6020	Shanghai Jinghong Experimental Equipment Co., Ltd.
Forced Air Drying Oven	DHG-9013A	Shanghai Yiheng Scientific Instrument Co., Ltd.
Centrifuge	TG16-WS	Shanghai Luxiangyi Instrument Co., Ltd.
Water Purification System	Master-S15 UV	Shanghai HoTech Company, China
Circulating Water Bath	CORIO CD-5	Beijing Youlaibo Technology Co., Ltd.
Fourier Transform Infrared Spectrometer	Nicolet 5700	Thermo Fisher Scientific China Co., Ltd.
Fully Automatic Physical Adsorption Analyzer	ASAP 2020M	Micromeritics (Shanghai) Instrument Co., Ltd.
Scanning Electron Microscope	FEI Verios 460L Regulus 8100	Thermo Fisher Scientific China Co., Ltd.
X-ray Diffractometer	MiniFlex600-C	Rigaku Corporation, Japan
Ultrasonic Cleaner	KQ-100VDV	Kunshan Ultrasonic Instrument Co., Ltd.
UV-Visible Spectrophotometer	UV-1700	Shimadzu Corporation, Japan

2.3 Preparation of MOFs

2.3.1 UiO-66(Zr)

UiO-66(Zr) metal-organic frameworks (MOFs) were synthesized via a solvothermal method, involving the heating of solutions containing zirconium salts, the corresponding acid form of the organic linker, and a modulating agent, formic acid. All starting materials and solvents, unless otherwise specified, were used without further purification. For the procedure of synthesizing, terephthalic acid (0.02898 g) and zirconium oxychloride octahydrate (0.0575 g) were dissolved in a solvent mixture comprising N, N-Dimethylformamide (DMF) and formic acid. The ratio of DMF to formic acid was maintained at 8.75 mL/2 mL in a 60-mL screw-capped glass jar[22]. The resulting mixture was heated to 120°C and maintained at this temperature for 24 hours under solvothermal conditions. After the solvothermal reaction, octahedral colorless crystals of UiO-66(Zr) MOF were obtained. The synthesized MOF was then washed twice with 5 mL of fresh DMF to remove any residual impurities, also the washing process involved centrifugation to separate the solid MOF product from the solvent. Subsequently, the as-synthesized sample of MOF- UiO-66(Zr) was rinsed three times with

10 mL of anhydrous DMF via centrifugation to further purify the material. The solid was dried at 80 °C under vacuum for 24 hours to yield the activated sample of UiO-66(Zr) MOF.

2.3.2 MIL-100(Fe)

The process of synthesis involves dissolving trimesic acid (H3BTC) (0.210 g, 210.14 mw) and ferric chloride hexahydrate (FeCl3·6H2O) (0.370 g, 270.30 mw) in 20 mL of N, N-dimethylformamide (DMF) solution while swirling magnetically for three to five minutes. After that, the mixture was poured into a 100 mL polytetrafluoroethylene liner. After that, the solution-containing liner was put in a stainless-steel reactor and aged for 24 hours at 150°C in a solvothermal oven.[23] To get rid of any remaining contaminants, the product was successively washed three times with ethanol and DMF following the solvothermal process. Centrifugation was used in the washing procedure to separate the solid MOF product from the solvent. After that, ethanol completely replaced the DMF in the solid. The MIL-100(Fe) MOF obtained was subjected to vacuum drying at 80°C for 24 hours to remove any remaining solvent and yield the final product.

2.3.3 ZIF-8

At room temperature (~25 ± 2 °C), 293 mg of zinc acetate dihydrate (Zn(OAc)2) was dissolved in 10 mL of deionized water (DI water) without stirring. In a different solution, 4.6 g of 2-methylimidazole (Hmim) was dissolved in 20 mL of DI water. Then, without stirring, the zinc acetate dihydrate solution was added to the 2-methylimidazole solution, keeping the molar composition of Zn/Hmim/water = 1/35/1280[24]. The resultant combination was allowed to mature at room temperature for a full day. Following aging, the precipitate was centrifuged for ten minutes at 8000 rpm in order to remove it from the colloidal dispersion. To get rid of any contaminants, the separated precipitate was washed three times with methanol. In order to prepare them for further characterization, the final products were dried in a vacuum oven at 60˚ C for 24 hours.

2.3.4 Al-fum

2.45 g of aluminum chloride hexahydrate, 1.4 g of fumaric acid, and 50 ml of N, N dimethylformamide (DMF) are combined in a beaker to start the process. After that, this mixture is heated to 130 °C while being constantly stirred for 96 hours. A centrifuge is used to separate the suspension after the reaction time, separating the solid precipitate from the liquid solution. To get rid of contaminants, the resultant precipitate is thrice washed with acetone and methanol. Then, to get rid of any last traces of solvent, the purified material is dried in an oven at 80 °C. Lastly, the white powder is heated for six hours at 60 °C in a vacuum oven to activate it[25]. This procedure guarantees that the appropriate material is prepared and purified for further use.

2.4 Characterization

2.4.1 X-Ray Diffraction (XRD)

Diffraction of X-rays A diffractometer (MiniFlex600-C, Rigaku Corporation, Japan) operating at 40 kV and 40 mA was used to capture XRD patterns with a Cu target K α radiation λ = 1.54056. At a scan rate of 10°/min and a step size of 0.01°, the XRD scans were carried out in the 5° to 50° range. The crystalline structure and phase composition of the material are revealed by XRD examination. including details on atomic locations, crystal symmetry, and unit cell characteristics.

Scanning Electron Microscopy (SEM)

Using a SEM (FEI Verios 460L, Thermo Fisher Scientific, China Co., Ltd.), the surface morphologies, form, size, and elemental compositions of pristine, after adsorption, and after improved coagulation were investigated for UiO-66(Zr), MIL-100(Fe), ZIF-8, and Al-fum. MOF samples are coated with gold prior to analysis in SEM characterization to improve conductivity and lessen charging effects during imaging. Along with preventing contamination, shielding sensitive samples from electron beam damage, and enhancing resolution and contrast, this coating also ensures more accurate and trustworthy analysis overall.

2.4.2 N_2 Sorption

Based on adsorption data, the surface area of the synthesized MOFs (UiO-66, MIL-100 Fe, ZIF-8, and Al-fum) samples was calculated using the Brunauer–Emmett–Teller (BET) technique. The material's particular surface area and pore structure are disclosed by the BET study. The isotherms for the adsorption and desorption of nitrogen were measured at 77 K utilizing an ASMAP 2020M BET analyzer from Micromeritics (Shanghai) Instrument Co., Ltd. Degassing was carried out at 120 °C under vacuum conditions for 48 hours before to the N2 absorption studies in order to remove any extraneous gases or vapors adsorbed on the surface of the MOF samples that may have affected the accuracy of the results. The nitrogen volumes that were adsorbed or desorbed were monitored by the Auto-Sorb device at relative pressures between 0.001 and just about 1.0. Through the examination of the N2-assisted adsorption-desorption data, the pore volume, and specific surface area. Under saturated circumstances, the isotherm measurements usually assess the materials' entire pore volume. When a notable rise in saturated pressure is noted, macro pores may be identified.

2.4.3 Fourier Transform Infrared Spectroscopy (FT-IR)

Thermo Fisher Scientific China Co., Ltd.'s Nicolet 5700 was used to perform Fourier transform infrared (FT-IR) spectroscopy in the 4000-400 cm-1 range. The purpose of this investigation was to characterize the various functional groups that make up the MOFs.

2.5 Adsorption

2.5.1 Calibration curve

A stock solution of humic acid was prepared by dissolving 1 g of humic acid in 62.5 mL of 0.1 M NaOH solution (added to ensure complete dissolution of HA), followed by dilution with distilled water to obtain a final volume of 1 L. This stock solution was further diluted for use in the experiments. During the experiments 3L of HA stock solution been used.

The calibration curve for Humic Acid (HA) concentration was established through a meticulous process as shown from Figure 1, beginning with the preparation of seven 250 mL flasks, each containing different concentrations of HA (1, 3, 5, 10, 30, 50, 100 mg/L) mixed with 80 mL of purified water. preparation of HA experiment conducted in a thermostatic shaker operating at 400 rpm. This setup ensured a range of HA concentrations to accurately define the relationship between concentration and absorbance. The entire procedure was conducted at a controlled temperature of 305°K to maintain consistency and prevent temperature-induced variability in the readings.

The collected absorbance data at 321 nm for each known HA concentration served as the foundation for plotting the calibration curve. By graphing the absorbance (A.u.) against HA concentration (mg/L), a linear relationship was established, indicated by the linear regression equation and the statistical parameters derived from it. This calibration curve is a critical tool for determining unknown HA concentrations in samples by comparing their absorbance values at 321 nm against the curve, leveraging the direct proportionality between HA concentration and its absorbance as dictated by the Beer-Lambert Law.

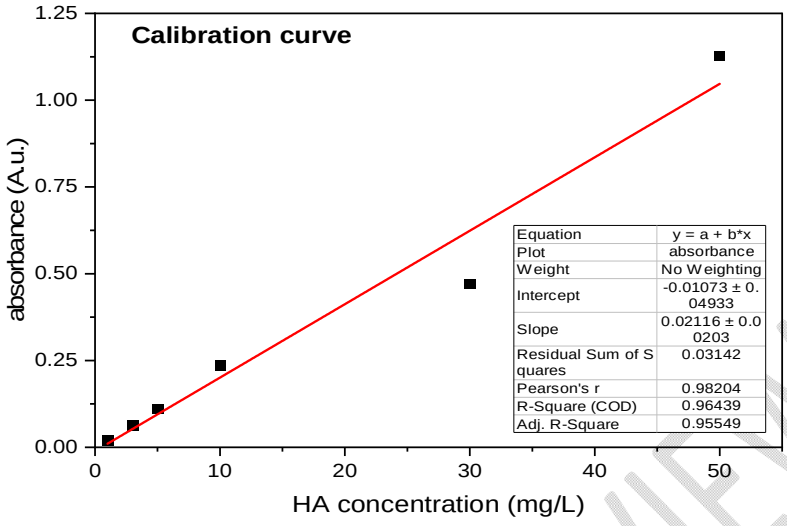

Figure 1. Calibration curve for determination of humic acid

2.5.2 Adsorption experiment

At 400 rpm, kinetic adsorption tests were carried out in a thermostatic shaker. For each experiment, 250 mL Erlenmeyer flasks containing 80 mL of HA solution and 40 mg of the corresponding MOFs were utilized. 0.1 M HCl or NaOH solution was used to change the HA solution's starting pH. HI 8424 pH meters were used to record pH readings. Contact time was changed at 0min, 3min, 5min, 10min, 20min, 30min, 1h, 1.5h, 2h, 4h, and 8h while maintaining the HA content at 50 ppm, temperature at 305 K, and pH at 6 in order to assess the kinetics and equilibrium time for HA adsorption [26].

By changing the initial pH of the solution from 4 to 8 while keeping the temperature constant at 305 K, the impact of pH on the adsorption of HA was examined. Contact time was used as the equilibrium time for each MOF as follows: HA concentration of 50 ppm, 240 min for Al-fum, 120 min for MIL-100(Fe), 120 min for ZIF-8, and 60 min for UiO-66(Zr). In an effort to determine the optimal pH removal for every MOF. In order to perform isotherm adsorption experiments, the HA concentration was varied from 1 ppm to 300 ppm at a constant temperature of 305 K and pH 6. The equilibrium contact time for each MOF was 120 min for MIL-100(Fe), 240 min for Al-fum, and 120 min for ZIF-8. and 60 min for UiO-66(Zr).

Unfiltered water samples from every MOF adsorption experiment were gathered and centrifuged in order to create the dry MOF samples. The samples were centrifuged, and then they were vacuum-dried for six hours at 80°C. The samples were subjected to XRD, FTIR, and SEM characterization after drying.

After each adsorption experiment, the solution was filtered using Whatman filter paper No. 41. The initial and residual HA concentrations were analyzed using a UV-Vis spectrophotometer (SHIMADZU COPRPORATION, UV-2600, JAPAN) at a wavelength of λmax = 321 nm. The absorbance was then compared with a calibration curve to determine the respective HA concentrations in the solution and the volume solution for each MOFs with different parameter been through centrifugation, then dried at 80C degree for 24 hours, as dry MOF samples for characterization of XRD, SEM, and FTIR.

Evaluation of Uptake Capacity (q): The uptake capacity ('q') represents the amount of humic acid (HA) adsorbed per unit mass of Co-MOF (mg/g). It was evaluated using the following Equation 2.1:

$$q = \frac{(C \circ - Cf)V}{m} \qquad 2.1$$

Where:

- C_o (mg/g) is the initial concentration of HA.
- Cf (mg/g) is the final concentration of HA.
- V (L) is the volume of the humic acid solution.
- m (g) is the adsorbent dosage of Co-MOF.

Different kinetics and isotherm models were fitted to the experimental adsorption data in order to suit the data. These models aid in comprehending the underlying mechanics and offer mathematical explanations of the adsorption behavior.

Adsorption Mechanisms: Predicting the effectiveness of the adsorption process and improving it both depend on an understanding of the adsorption mechanism. Various kinetics and isotherm models may be fitted to experimental data to gain understanding of the adsorption mechanisms.

Models of Kinetics and Isotherms: The adsorption process may be explained by a variety of isotherm and kinetics models. Table 1 contains the typical equations for the various models. Kinetics models explain the rate of adsorption over time, whereas isotherm models explain the equilibrium connection between the adsorbent and adsorbate at a fixed temperature.

Pseudo-first-order kinetic model Equation 2.2:

$$ln(Q_e - Q_t) = lnQ_e - k_1 t \qquad 2.2$$

Pseudo-second-order kinetic model 2.3:

$$\frac{t}{Q_t} = \frac{1}{k_2 Q_e^2} + \frac{t}{Q_e} \qquad 2.3$$

where Q_e (mg g^{-1}) is the equilibrium adsorption capacity of the MOFs, Q_t (mg g^{-1}) is the adsorption capacity at time t (min), k_1 (min-1), k_2 (g min^{-1} mg^{-1}), and kid (mg g^{-1} $min^{-0.5}$) are rate constants of pseudo-first order models, pseudo-second-order. The isotherm adsorption data was fitted with the following adsorption isothermal models:

Langmuir isotherm model Equation 2.4:

$$\frac{C_e}{Q_e} = \frac{1}{bQ_{m.1}} + \frac{C_e}{Q_{m.1}} \qquad 2.4$$

Freundlich isotherm model Equation 2.5:

$$lnQ_e = lnk_f + \frac{1}{n} lnC_e \qquad 2.5$$

where Ce (mg L^{-1}) is the equilibrium concentration of HA, b (L mg^{-1}) and Qm,1 (mg g^{-1}) are the Langmuir constant and the monolayer adsorption capacity, respectively; n and KF [(L mg^{-1})$^{1/n}$ mg/g] are related to adsorption intensity and capacity

3 Result and discussion

3.1 Characterization

3.1.1 Crystal structure by XRD

Changes in anion composition were reflected in peak shifts in X-ray diffraction (XRD) patterns, suggesting modifications to the synthesized MOFs' molecular structure as seen inFigure 2. These patterns closely match their simulated single-crystalline XRD profile, verifying the synthesized MOF materials' structural integrity and resemblance to the known bulk crystalline framework.

Due to its stable Zr-based MOF structure, UiO-66(Zr) is projected to have a high degree of crystallinity, as evidenced by its sharp peaks. The simulated pattern is closely matched by peaks at 2θ = 7.5 and 8° values, which validate the effective synthesis of the UiO-66(Zr) framework. The framework has distinct pore diameters and a metal-ligand coordination geometry. Notably, a shift in the peak at 2θ = 7.5 and 8° towards lower angles was detected on the UiO-66(Zr) XRD graph, indicating a subsequent expansion in the lattice gap. This change emphasizes the impact of nitrate ions on the UiO-66(Zr) structural characteristics, emphasizing its malleability and the possibility of chemically modifying it to get customized porosity.

Moreover, MIL-100(Fe) exhibits distinct, sharp peaks that point to a pure phase with exceptional crystallinity. The simulated pattern alignment indicates that the Fe centers and

organic linkers are suitably synchronized, leading to the creation of the recognizable large pores in MIL-100. Interestingly, when the concentration of NO3 ions rose, a noticeable shift in the peak within the 2θ range of 10–12° towards lower angles was seen. This change, which suggests that the addition of NO3 ions directly affects the structural properties of MIL-100(Fe), may allow for controlled alteration of its porosity and interstitial features. It also indicates an expansion in the lattice spacing.

Its high crystallinity, characteristic of ZIF materials, is confirmed by the ZIF-8 pattern with sharp peaks. The Zn (II) ions and imidazolate linkers create the predicted sodalite-type structure with homogeneous microporous cavities, according to the match with the simulated pattern. The pattern shows clear, sharp peaks that are a sign of crystallinity. The X-ray diffractograms showed sharp diffraction peaks at 7.4°, 12.7°, and 18°. In particular, the strong peak at 7.4° validates that ZIF-8 has been successfully synthesized.[27, 28]

The corresponding simulated and synthesized patterns of Al-fum show that the material was successfully synthesized in accordance with its anticipated crystalline structure. 10°C is the observed

high. Little peaks, however, are also seen at greater angles, which may indicate the existence and strength of Al ions.

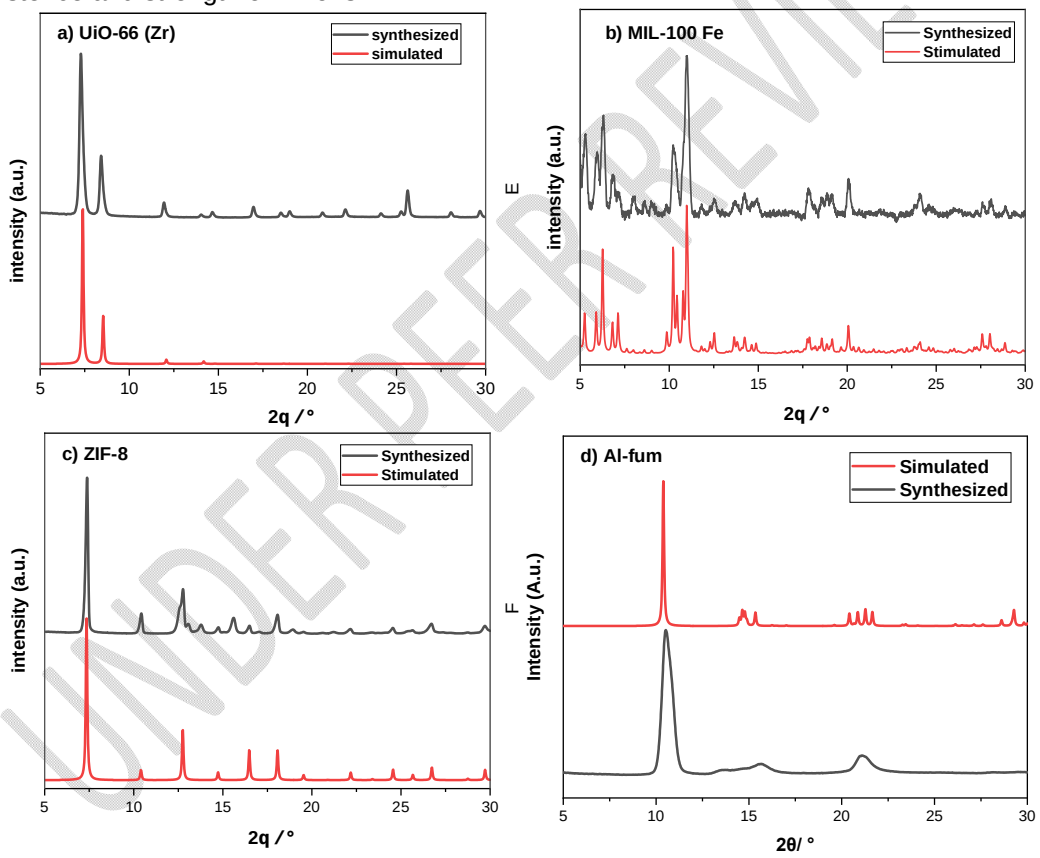

Figure 2. PXRD patterns for a) UiO-66 (Zr), b) MIL-100 Fe, c) ZIF-8, d) Al-fum

3.1.2 Textural properties by N2 sorption

Figure3provides a detailed assessment of the MOFs' performance and features with regard to their ability to adsorb nitrogen (N2). The surface area and porosity of the MOFs are revealed by the data from the Brunauer-Emmett-Teller (BET), Langmuir surface area, and total pore volume measurements shown inTable3.

With a Langmuir surface area of 1514 m^2/g and a BET surface area of 1378 m^2/g, UiO-66(Zr) has a large surface area that suggests its potential for use in gas adsorption and catalytic applications. Heterogeneity in pore sizes or shapes is suggested by the discrepancy between BET and Langmuir surface areas. With a total pore volume of 0.56 cm^3/g, UiO-66(Zr) demonstrates a modest pore volume, which contributes to its respectable adsorption ability for smaller molecules. Its zirconium centers give it structural stability even if its pore capacity isn't the largest, which enables it to preserve its integrity under extreme heat and chemical stress and retain constant adsorption performance. The pore aperture, or pore size, is around 6-7 Å, which corresponds to the benzene ring's size[29]. The amount adsorbed increases steadily as relative pressure rises on the N2 isotherm graph of UiO-66(Zr), with a small curve before reaching a plateau. The curve points to a Type I isotherm, which is typical of materials with microporous structure. The presence of micropores where nitrogen molecules are swiftly adsorbed is shown by the adsorption curve's fast rise at low relative pressures. With minimal hysteresis and a trajectory resembling the adsorption curve, the desorption curve indicates that network effects and pore obstruction are not a major concern and that the pores are accessible.

With a Langmuir surface area of 2013 m2/g, MIL-100(Fe) has a high BET surface area of 1600 m2/g. This indicates a very high porosity and potential use in situations where the greatest possible surface contact is needed, such as catalysis or high-capacity gas storage. MIL-100 Fe has a total pore volume of 0.56 cm^3/g, which is comparable to UiO-66(Zr) and supports a moderate adsorption capability. But unlike UiO-66(Zr), it is particularly well adapted for the adsorption of bigger molecules like benzene and other aromatic compounds because of its iron-based composition and bigger pore size. The iron(III) carboxylate material MIL-100(Fe) has bigger pore diameters of around 25–27 Å, or about the size of a benzene molecule[30]. The MIL-100(Fe) N2 isotherm curve shows a type IV isotherm with a hysteresis loop, which is usually connected to mesoporous materials. Mesoporous materials are indicated by the adsorption curve's sharp rise at modest relative pressures. For materials containing mesopores and capillary condensation, the desorption curve typically forms a hysteresis loop. This suggests that compared to UiO-66(Zr), the pores are bigger.

ZIF-8 has the largest Langmuir surface area of 2002 m2/g, with its BET surface area of 1820 m2/g following closely behind. This suggests a very consistent and easily accessible pore structure, making it perfect for gas separation applications where pore size and shape uniformity is essential. With a total pore volume of 0.81 cm^3/g, ZIF-8 has the most potential of all the other compounds to host a greater volume of adsorbates. Pore diameters of ZIF-8, a cobalt(II) benzene-dicarboxylate substance, are around 10 Å[31]. The isotherm graph of ZIF-8 displays a type I isotherm with separate adsorption and desorption curves that is comparable to UiO-66(Zr). Micropores are present because the adsorption curve grows quickly at low relative pressures. With little hysteresis, the desorption curve closely resembles the adsorption route, indicating effective adsorption and desorption with no appreciable pore obstructions.

With a BET surface area of 1118 m^2/g and a Langmuir surface area of 1262 m^2/g, Al-fum has the lowest surface area values of all the materials. This suggests that it may have bigger, less accessible pores or a denser structure. Pore Volume Total: 0.70 cm^3/g. Due to its comparatively large pore capacity, al-fum has tremendous promise for uses like hazardous waste removal and water purification that need for strong adsorption properties. The organic fumarate connections provide diverse chemical activity that may be utilized in selective adsorption procedures, while the aluminum centers serve as strong points of contact for contaminants[32]. Al-fum's isotherm shows a mix of type I and IV properties, including some mesoporous and microporous elements. At low pressures, the curve rises rapidly, showing microporous adsorption; at higher pressures, the curve increases more gradually, revealing the existence of some mesopores. A hysteresis loop in the desorption curve indicates capillary condensation inside the mesopores.

When the four materials are compared, ZIF-8 and UiO-66(Zr) both exhibit type I isotherms that are suggestive of microporous structures. They also have minimum hysteresis, which signals effective pore accessibility and little blocking effects. Mesopores are seen in MIL-100(Fe) and Al-fum, which show type IV isotherms with hysteresis loops. Compared to Al-fum, MIL-100(Fe) displays a more noticeable hysteresis loop, which may indicate bigger mesopores or more intricate pore architectures. Al-fum's isotherm shows that at higher pressures, mesopore filling occurs after initial micropore filling, demonstrating a mix of microporous and mesoporous behavior. Applications needing a high micro-porosity are better suited for materials like ZIF-8 and UiO-66(Zr). Because of their mesoporous architectures, MIL-100(Fe) and Al-fum could be more appropriate for uses where bigger pore sizes are required for molecule diffusion or storage.

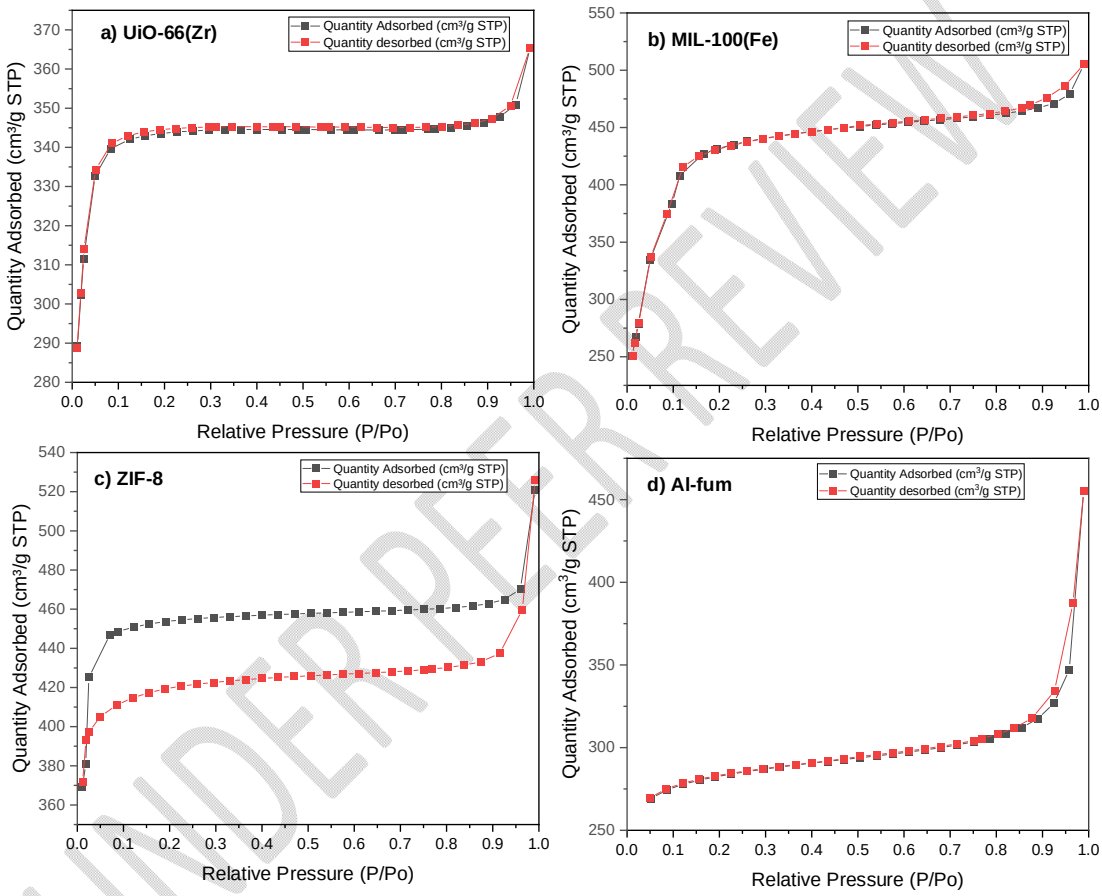

Figure3. N_2 adsorption/desorption isotherms of a) UiO-66(Zr), b) MIL-100(Fe), c) ZIF-8, d) Al-fum

Table3. Porous properties for the synthesized MOFs

MOF	Surface area m^2/g		Total pore volume cm^3/g
	BET	Langmuir	
UiO-66(Zr)	1378	1514	0.56
MIL-100(Fe)	1600	2013	0.56
ZIF-8	1820	2002	0.81

Al-fum	1118	1262	0.70

3.1.3 Morphology by SEM

UiO-66(Zr) morphology generally shows a very regular, octahedral shape that is constant across the variety of pictures supplied by image (a,b) inFigure 4. The Zr6O4(OH)4 clusters and the way the organic linkers (1,4-benzenedicarboxylate, BDC) connect these clusters to form the framework's overall cubic structure directly result in the octahedral shape. Lower magnifications of Image (a) reveal a high density of particles that are largely consistent in size and shape. The sample appears to have a large surface area, which is a desired property for MOFs utilized in gas storage or catalysis, as shown by the closely packed particles. Close-ups of individual crystals are shown in image (b), where the geometric regularity and edge sharpness are clearly visible. The smooth surfaces indicate a high degree of purity and crystallinity in the synthesized material, since there are no obvious faults or impurities.

The consistent size and characteristic octahedral shape of UiO-66(Zr) particles, which are indicative of high-quality crystals, are highlighted in the SEM pictures. This regularity in shape points to a well-managed synthesis process with few contaminants. Zr6O4(OH)4 clusters act as nodes in the composite, whereas BDC ligands act as linkers. This interaction between the composite and ligands is critical. Because of this configuration, the structure is very porous and has strong Zr-O bonds, which provide chemical and thermal stability. All in all, these features point to an efficient synthesis methodology that should provide outstanding results in real-world uses.

As can be seen from image (c,d) of Figure 4, SEM images of MIL-100(Fe) reveal a polyhedral shape with a somewhat uniform size distribution. We can estimate the size of the particles, which seem to be in the micrometer range, thanks to the magnification. Well-formed MOFs are characterized by a high degree of crystallinity, which is suggested by the smooth faces and edges.

Image (c) makes it easier to see how the crystals' unique shapes. Their smoother surfaces appear to preserve the same polyhedral geometry, suggesting a regulated synthesis process and a constant development pattern. A cluster of crystals appears to be depicted in picture (d). While some of the crystals have distinct forms, others lack them, maybe as a result of partial crystallization or aggregation.

In conclusion, MIL-100(Fe) appears to have been synthesized with some degree of size and shape homogeneity, which is indicative of a carefully managed synthesis process, according to the SEM pictures. The crystal surface's striations and layers might indicate that various facets have varying growth speeds, which could be affected by ligands during synthesis.

ZIF-8 generally displays a rhombic dodecahedral shape, as seen in Figure 4 picture (e,f). The sodalite-type framework's intrinsic symmetry, which directs crystal formation in twelve comparable rhombic faces, is directly responsible for this.

Individual rhombic dodecahedrons are easier to see in picture (e). The continuous growth rate on all crystal facets is suggested by the uniform size and shape, indicating regulated synthesis conditions. The particles in picture (f) have smooth surfaces and distinct, crisp geometric features, which suggests that the synthesis was done in a way that encourages great crystallinity.

ZIF-8 particles with sizes ranging from tens of nanometers to a few micrometers are seen in the SEM photos. These particles have a constant rhombic dodecahedral form. The ideal packing density in storage and separation applications is made possible by this form. By serving as nodes between imidazolate linkers, zinc ions form a robust structure that is resistant to collapsing when guest molecules, such as solvents, are removed.

The uniform morphology observed in every picture point to a well-regulated synthesis process, where variables like as solvent, temperature, time, ligand to metal ratio, zinc supply, and solvent are all tightly controlled. The excellent crystals that were seen show that these

parameters were precisely controlled, producing a product with exceptional structural integrity, purity, and crystallinity.

Particles from Figure 4 with an uneven, somewhat flaky morphology are seen in Image (g) of Al-fum. It seems like a collection of layered structures that are loosely aggregated rather than a uniform shape. The particles show a wide range of sizes and don't seem to follow any particular geometric design. A closer view of the particles is provided by Image (h), which confirms their flaky, uneven appearance.This is when the layers become more noticeable, and we can see how the flakes build atop one another to form a more intricate pattern. This kind of morphology might be a sign of a synthesis procedure that encourages the development of plates or sheets, thus adding to a large surface area that is advantageous for adsorption and catalysis applications.

The Al-fum particle SEM pictures show a heterogeneous distribution of sizes, ranging in size from sub-micrometer to micrometer. This difference is typical of some synthesis techniques where uniform particle size is not as important as attributes like surface area. picture (g) clearly shows a es a deeper examination of specific particle particles display a textured and rough surfa e of a high level of porosity that is frequently hat the particle surface has many nooks and a for molecular interactions during adsorptio reveals flaky particles with layered structure the heterogeneous surface texture. This in tegy that gives priority to surface-related s ability to operate, such catalytic activity ures show Al-fum particles with complex su emphasizing that even with their diverse mor procedures.

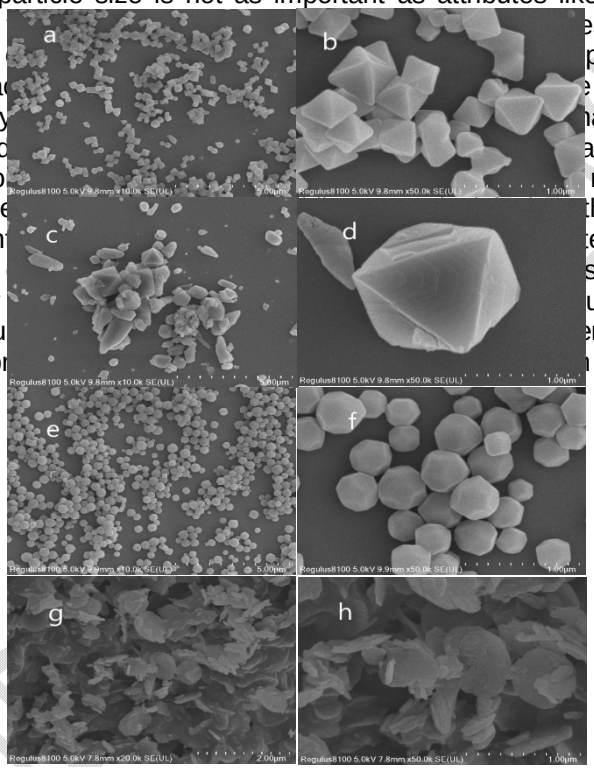

Figure 4. SEM images of (a,b) UiO-66(Zr), (c,d) MIL-100)Fe), (e,f) ZIF-8, (g,h) Al-fum in pristine state

3.1.4 Chemical structure by FTIR

FTIR spectra fromFigure5 (a) showed UiO-66(Zr) peak shifts, which further supported the structural synthesis of UiO-66 (Zr) MOF. Noted O-H stretching vibrations, which are suggestive of moisture or hydroxyl groups inside the framework, are suggested by peaks at 3673.8 cm^{-1}. Band at 1506.5 cm^{-1}: Usually terephthalic acid in UiO-66(Zr) is the organic linker's aromatic C=C stretching vibrations. Peak of 739.3 cm^{-1}, typical of Zr-O stretching, indicating the composition and structure of the metal-organic framework. Wide band at 3400 cm^{-1}indicates an O-H extending from hydroxyl or water units. Peak at 1587 cm^{-1} most likely corresponds to the C=O stretching vibration, which is in line with UiO-66(Zr)'s terephthalate ligands. The fingerprint area (below 1000 cm^{-1}) for distinctive peaks highlights the Zr-O bonds, which are essential for the UiO-66(Zr) framework.

The FTIR spectra presented in Figure 5 (b) showed MIL-100(Fe) peak shifts, which further supported the structural synthesis of MIL-100 Fe MOF. O-H stretching may be the cause of the faintly visible peaks at 3674 cm^{-1} and 3610 cm^{-1}, which are less noticeable because of the structure of the material. The existence of carboxylate groups is suggested by the distinct peak at 1384.6 cm^{-1}, which shows how the organic linker interacts with iron. Peaks at and below 750 cm^{-1} are indicative of Fe-O vibrations and are consistent with the structure predicted for MIL-100 Fe. wide peak around 3400 cm^{-1} Comparable to Al-fum, but with hydroxyl groups or water content indicated. Carboxylate groups (COO-) may be stretched symmetrically and asymmetrically to produce distinct peaks at around 1600 cm^{-1} and 1384 cm^{-1}. reacting with the trimesate ligands that are frequently connected to MIL-100 Fe. Fe-O bonds are shown by peaks about 800-600 cm^{-1}, and these bonds are essential to the MOF's structural stability. The presence of Fe (II) in the samples was confirmed by the FTIR spectra, which displayed a clear peak shift between 711 cm^{-1} and 1385 cm^{-1} in MIL-100(Fe). This shift suggested a modification in the coordination environment or bond strength of the Fe (II) ions in the samples. when the metal ions' oxidation state changes, like in this instance when Fe (III) is reduced to Fe (II).

ZIF-8 Peak shifts were seen in Figure 5 (c) FTIR spectra, adding more evidence to support the structural synthesis of ZIF-8 MOF. Less prominent than in Al-fum, the broad peak at 3400 cm^{-1} suggests a lower hydroxyl or water content. The C=N stretching vibrations from the imidazole ring, which correspond to peaks at 1584 cm^{-1} and 1146.8 cm^{-1}, are essential for determining the identity of the organic linker in ZIF-8. incisive Peaks that are less than 1000 cm^{-1} confirm the existence of imidazolate linkers linked to zinc by indicating the presence of Zn-N coordination bonds. The absence of large O-H stretching peaks at 1580 $cm^{-1}$and below compared to the other peaks may imply a lower water content or greater binding within the framework. Peaks in this area correspond to imidazolate linkers, more especially to C-N stretching and bending vibrations, which show the structure of ZIF-8. Within the imidazolate framework, a characteristic fingerprint area indicates the Zn-N coordination.

FTIR spectra from Figure 5 (d) showed Al-fum peak shifts, confirming the structural synthesis of Al-fum MOF. O-H stretching from hydroxyl groups or water molecules in the structure is shown by a broad band about 3400 cm^{-1}. Peaks seen at 1619.3 cm^{-1} and 1424.2 cm^{-1} are compatible with the fumarate anions in Al-fum and are indicative of symmetric and asymmetric stretching vibrations of carboxylate ions (COO-) connected to metal ions. Metal-oxygen vibrations, which are characteristic of MOFs, are seen in the fingerprint area below 1000 cm^{-1}, confirming the metal-ligand coordination. O-H stretching vibrations are most likely responsible for the broad peak observed at 3400 cm^{-1}. This indicates the presence of water

molecules or hydroxyl groups within the MOF structure, which is typical of MOFs because of their porous nature, which attracts water. Sharp peaks in the 1600–1400 cm^{-1} range correspond to the predicted fumarate ligands in Al–fum and are usually suggestive of C=O stretching vibrations. Metal-oxygen (M-O) vibrations are typified by peaks around 800-400 cm^{-1}, which validate the metal-ligand coordination framework that is necessary for the stability of the MOF structure.

HA the FTIR spectra from Figure 5 (e) showed peak changes, which further supported the structural humic acid (HA) hypothesis. noted a wide Peak at 3600-3200 cm^{-1}, which is indicative of O-H stretching vibrations from alcohols and carboxylic acids, suggests that these functional groups, which are common in humic compounds, are present. Humic acid's aliphatic character is demonstrated by the peak about 2920 cm^{-1} which is due to C-H stretching vibrations from methylene groups. The complex character of humic compounds with different functional groups is highlighted by strong peaks at 1619 cm^{-1} and 1247 cm^{-1}, which correspond to C=O stretching in carboxylic groups and C-O stretching vibrations in phenolic ethers, respectively.

Additional evidence for the structural integrity of Kaolin was provided by the observation of peak changes in the FTIR spectra from Figure 5 (f). O-H stretching vibrations from hydroxyl groups inside the kaolinite structure, notably in the alumina sheets, are responsible for the peaks at 3697 cm^{-1} and 3620 cm^{-1}. The Si-O stretching vibrations that correlate to the Sharp Peak at 1032 cm^{-1} are indicative of the silicate layers in kaolinite. Al-Al-OH bending vibrations often have a peak at 914 cm^{-1}, which further verifies the mineral's composition.

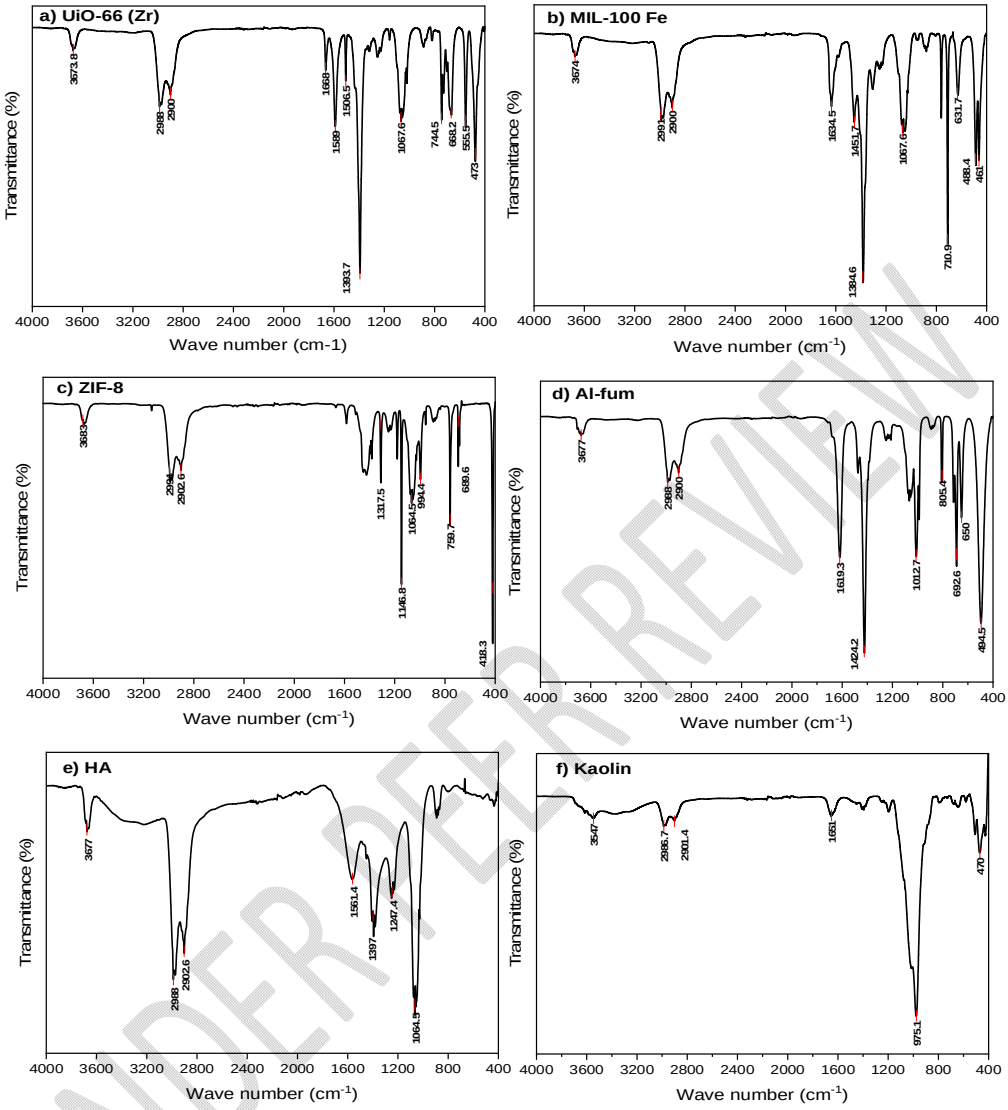

Figure5. FT-IR spectra of a) UiO-66(Zr), b) MIL-100(Fe),c) ZIF-8, d) Al-fum, e) HA, f) Kaolin

3.2 Removal of humic acid by MOF adsorption

3.2.1 Kinetic adsorption

Figure 6 (a) shows the outcome of the investigation into the impact of contact duration on the adsorption of humic acid (HA) onto UiO-66(Zr). The adsorption of UiO-66(Zr) over time is shown in graph (a) to show a progressive decline in adsorption rate, signifying a change from fast adsorption to equilibrium. This implies that UiO-66(Zr) has a high affinity for compounds that adsorbate.

The strong Pearson correlation coefficient (0.99978) and R-square value (0.99956) of the pseudo-second-order kinetic model provide a good match to the experimental data, suggesting that the model can account for almost all of the variability in the adsorption data. The model's remarkable accuracy in characterizing the adsorption process is further supported by the very low residual sum of squares. A more favorable match with the pseudo-second-order model implies that chemical adsorption, or chemisorption, which

involves the sharing or exchange of electrons between UiO-66(Zr) and the adsorbate and relies on valence forces, might be the rate-limiting phase.

Table.4provides a summary of the kinetic data analysis findings. The best-fit model was identified by comparing the regression coefficients (R2) and residual sum of squares (RSS). It was discovered that the pseudo-first-order model and the experimental data did not have a strong linear connection. The strong Pearson correlation coefficient (0.99844) and R-square value (0.99608), on the other hand, show that the pseudo-second-order kinetic model fits the experimental data quite well and suggests that chemical adsorption is the primary mechanism controlling adsorption.

Figure 6(c) shows the findings of the investigation into the impact of contact duration on the adsorption of humic acid (HA) onto ZIF-8. Because there are a lot of potential active sites on ZIF-8, the steep first slope predicts a high adsorption rate at first. The rate drops over time as the active sites fill up and get occupied; this plateau signifies that equilibrium has been reached. After 60 minutes of equilibrium, the adsorption curve levels off at 70 mg/g.

The second-order model, which has a smaller residual and higher R-square and Pearson's r values, may more closely reflect the adsorption kinetics of ZIF-8, according to the comparison of the first and second pseudo-order kinetic models. The second-order model's improved fit may suggest that chemisorption—adsorption involving the creation of chemical bonds and other adsorbate-adsorbent interactions—is involved in adsorption.

Figure 6(d) shows the outcome of the investigation into how contact duration affects humic acid's (HA) adsorption over Al-fum. According to the graph, equilibrium is attained when the curve plateaus, meaning that the adsorption capacity does not significantly increase with time.

The pseudo-first-order kinetic model fits the Al-fum adsorption data somewhat better than the pseudo-second-order model, according to the statistical parameters. The adsorption kinetics of Al-fum under the experimental conditions appear to be more in line with a process in which the rate of occupancy of adsorption sites drops exponentially with time, based on the better fit of the pseudo-first-order model. This might point to a process dominated by physisorption, in which there are plenty of accessible sites at first, leading to a high adsorption efficiency, but this efficiency decreases as these sites are occupied.

Table.4 Fitting parameters of Pseudo-first-order, Pseudo-second-order

Adsorbent	C_0 (mg/g)	$q_{e,exp}$ (mg/g)	Pseudo-first-order model			Pseudo-second-order model		
			$q_{e,cal}$ (mg/g)	K_1 (1/min)	R^2	$q_{e,cal}$ (mg/g)	K_2 g/(mg · min)	R^2
UiO-66(Zr)	50	26.52	27.87	-0.0006	0.915	28.43	0.011	0.9998
MIL-100(Fe)	50	29.5	10.1	-0.0002	0.167	36.15	0.0024	0.996
ZIF-8	50	68	20.54	-1.53	0.053	70.27	0.00097	0.992
Al-fum	50	74.21	43.22	-6.41	0.8622	75.53	0.00086	0.998

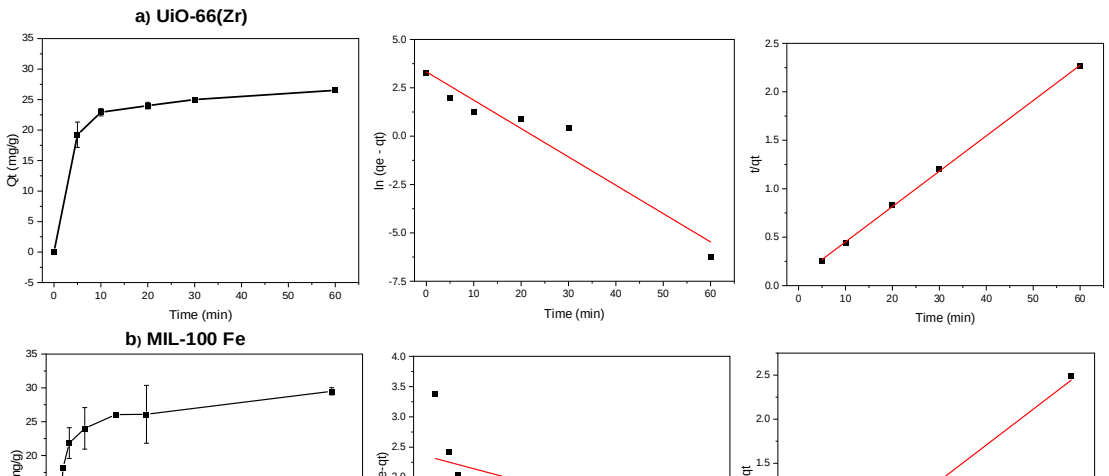

Effect of pH

Figure7shows the initial effect of pH variation on the adsorption capacity of UiO-66(Zr). At acidic pH (4-6), the initial observation shows that, in contrast to typical expectations, Qt is higher for UiO-66(Zr) in acidic conditions. This suggests that HA and the MOF have a

favorable interaction under these conditions. While HA is protonated in an acidic environment, this does not decrease its interaction with UiO-66(Zr); rather, it enhances some interactions with the terephthalate ligands or the zirconium nodes. It is possible that the presence of extra H+ ions will cause HA to become more compact or change in conformation, which will facilitate its interaction with the MOF. Furthermore, the ligands made of terephthalate may be better able to interact with HA via hydrogen bonding or other processes as a result of the modest protonation.

The iron trimer clusters in MIL-100 Fe are linked by tricarboxylate ligands, and because the metal centers are prone to hydrolysis, they may behave differently at different pH values. The higher Qt at pH 4 indicates that MIL-100 Fe adsorbs the intended adsorbate more successfully in an acidic environment. Numerous reasons, including as the protonation of carboxylate ligands and the increased electrostatic attraction between the negatively charged adsorbate molecules and the MOF, might be the cause of this.

When the pH is neutral, ZIF-8 usually exhibits the best adsorption capability, which is beneficial for preserving the chemical and structural stability of different adsorbates as well as the MOF. More efficient adsorption is made possible at pH 7, where the electrostatic interactions between ZIF-8 and the adsorbates are maximized with low repulsive forces. Interactions with adsorbates are facilitated by the neutrality, which also guarantees that the imidazolate linkers are in their most stable state. The absorption of HA rises with the pH of the starting solution and reaches a maximum value at pH 7, after which it starts to vary more quickly. The weakly acidic carboxylic and phenolic functional groups included in HA tend to ionize at pH values that are neutral or slightly acidic.

As can be seen from Figure7(d), the initial impact of pH varied on Al-fum's adsorption capacity. High Qt was seen at acidic pH (4 & 5), indicating that Al-fum has a high adsorption capacity for HA at higher acidic pH levels. This increased capability is explained by the dynamics of the interaction between the negatively charged HA molecules and the positively charged Al-fum sites, which are amplified in acidic environments because of protonation. Because of the acidic environment, carboxylic groups in HA become protonated, which may increase or neutralize negative charges and allow for a tighter contact with the metal sites of Al-fum. Furthermore, in acidic environments, Al-fum may have surface alterations that increase its affinity for HA.

The physicochemical characteristics of each MOF's metal centers and organic ligands, which affect the total charge, hydrophilicity, and accessibility of adsorption sites, are strongly related to the fluctuation in Qt across various pH levels. Higher pH values are clearly preferred by ZIF-8 and Al-fum, indicating that these compounds are better suited for adsorption in neutral to alkaline environments. While MIL-100(Fe) performs better in alkaline settings, UiO-66(Zr) seems to function best at pH values close to neutral. The fact that different MOFs have different ideal pH. for adsorption highlights how crucial it is to take the pH of the chemical environment into account when using MOFs for adsorption operations.

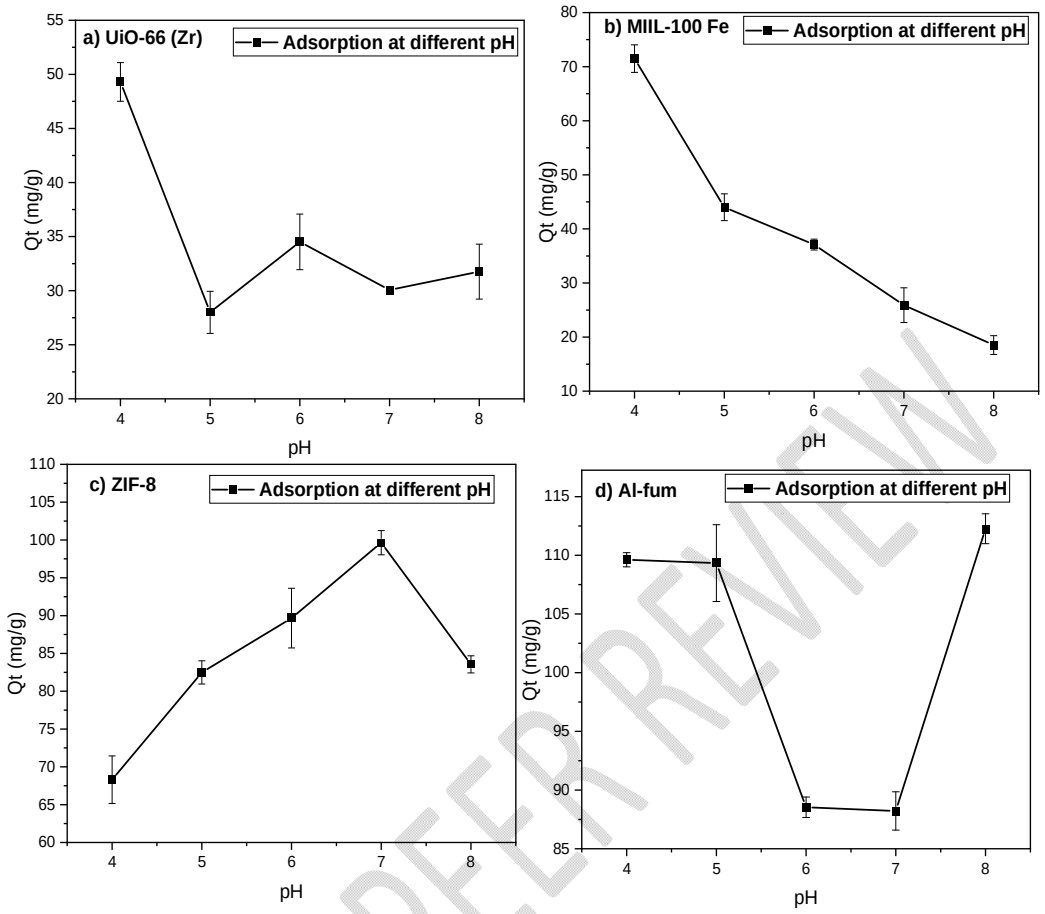

Figure7. Initial pH effect on adsorption capacity of a) UiO-66(Zr), b) MIL-100(Fe), c) ZIF-8, d) Al-fum MOFs (adsorbent dosage = 40 mg, volume = 0.08 L, initial concentration = 50 mg/L, temperature = 305 K, contact time= equilibrium time of each MOF)

3.2.2 Effect of adsorbent dosage on isotherm adsorption

The experimental data underwent nonlinear regression, resulting in the isotherm outcomes displayed inTable 5. The fact that the value Kf changes for every MOFs indicates that adsorption is endothermic. Table 6provides the model expression for both the kinetic and isothermal adsorption investigations.

The UiO-66(Zr) adsorption isotherm is shown in Figure8(a). For monolayer coverage, the Langmuir model assumes homogenous adsorption sites. Although not as high as some other MOFs, the q value indicates that UiO-66(Zr) has a high adsorption capacity, and the k value indicates a strong contact between the adsorbate and UiO-66(Zr). The 0.928 R-Square score suggests a better match.

The adsorption isotherm for MIL-100(Fe) has been obtained from Figure8(b). The maximal adsorption capacity (q = 129.45 mg/g) and the adsorption affinity constant (k = 0.128) define the Langmuir equation. This shows a reasonably good match, indicating that MIL-100(Fe) may contain bigger pores and iron-based clusters than UiO-66(Zr), perhaps leading to more uniform adsorption sites. On a homogeneous surface with a finite number of identical sites, monolayer adsorption is assumed by the Langmuir isotherm. A better match than the Freundlich model is suggested by the comparatively higher R-Square value (0.95), which shows that the actual adsorption behavior complies with the ideal monolayer assumption.

The adsorption isotherm for ZIF-8 is shown in Figure8(c). The numbers q=754 mg/g and k=0.0279, which denote the maximum adsorption capacity and the affinity between the adsorbate and adsorbent, respectively, define the Langmuir equation. Monolayer adsorption on a surface with finite, identical sites is suggested by this concept. ZIF-8 has a considerable adsorption capacity as indicated by the high q value, whereas the value of k shows a reasonably strong contact between ZIF-8 and the adsorbate. A multi-point adsorption method was used to adsorb HA onto the ZIF-8 surface, suggesting that the adsorption process occurred on a heterogeneous surface. Furthermore, the intensity of the interaction between the adsorbent and the adsorbate is indicated by the Kf value. An increased affinity between the two is indicated by a higher Kf value. The existence of tiny adsorbate molecules, which have easy access to the ZIF-8 material's micropores and cause adsorption on the surface as well as in extra-crystalline pores, is responsible for the Type I isotherm.

Al-fum's adsorption isotherm is shown in Figure8(d). According to the Langmuir model, monolayer adsorption occurs on a surface with a limited number of identical sites. Langmuir Model Fitting reveals that the Langmuir model fits the experimental data for Al-fum well, as seen by the high R-Square value (0.982). This implies that there is a maximum adsorption capacity and that the adsorption process closely resembles a monolayer adsorption mechanism with uniformly distributed surface sites.

To sum up, ZIF-8 is the best option for monolayer adsorption with uniform adsorption sites since it has the greatest R-Square value (0.997) for the Langmuir fit. This is in line with ZIF-8's structural features, which are distinguished by their homogeneous pore size distribution and large surface area.

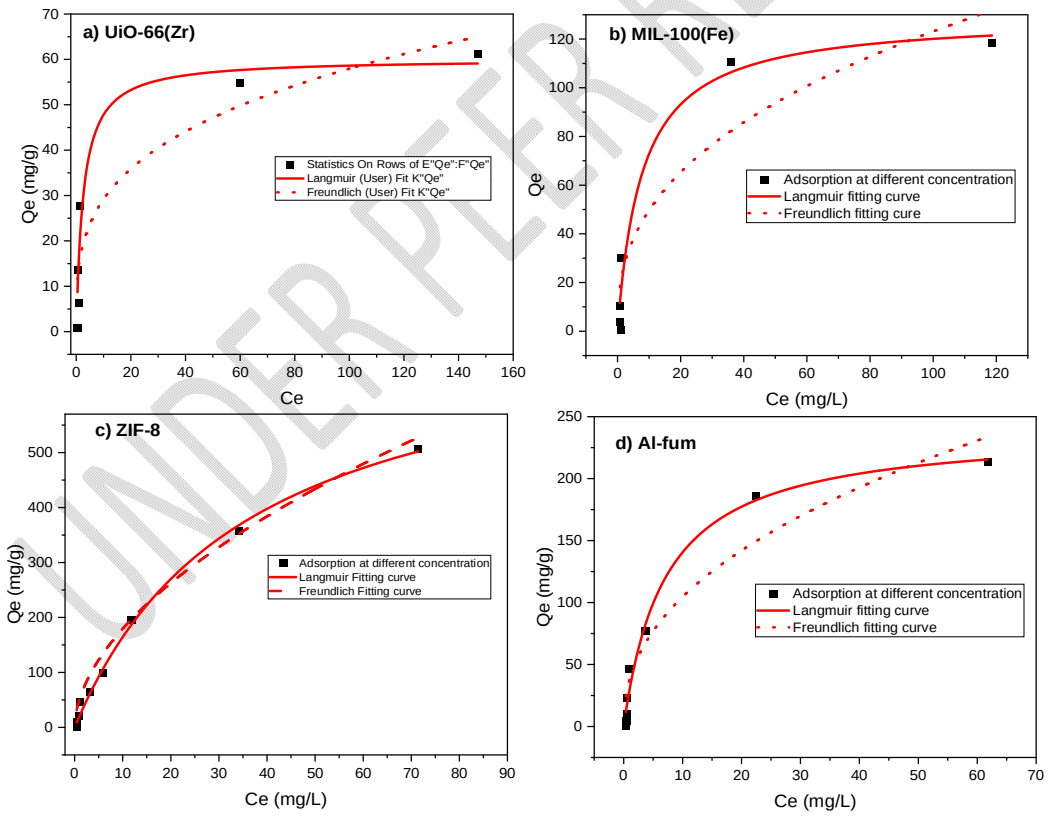

Figure8. Adsorption isotherm of a) UiO-66 (Zr), b) MIL-100 Fe, c) ZIF-8, d) Al-fum at (pH= best pH removal of its each MOFs, dosage= 40 mg, volume solution= 80 mL, temperature= 305 K, initial HA concentration= 50mg/l, contact time= equilibrium time of each MOF)

Table 5. Fitting parameters for Langmuir and Freundlich models

Adsorbent	Temperature (K)	Langmuir			Freundlich		
		q_{max} (mg/g)	K_L	R^2	K_F	n	R^2
UiO-66(Zr)	305	60.14	0.387	0.928	14.7	3.36	0.87
MIL-100(Fe)	305	129.45	0.128	0.95	20	2.53	0.855
ZIF-8	305	753.98	0.028	0.997	50.88	1.83	0.986
Al-fum	305	240.2	0.141	0.982	37.81	2.26	0.922

Table 6. Model expression s for kinetic and isotherm studies

Model/Function name	Expression	Parameters/Description
	Kinetic	
Pseudo first order model	$\ln (q_e - q_t) = \ln (q_e) - k_1 t$	q_e (mg/g), equilibrium adsorption uptake q_t (mg/g), instantaneous adsorption uptake k_1 (1/min), pseudo first order rate constant
Pseudo second order model	$t/qt = 1/K_2 qe2 + 1/qet$	k_2 (g mg–1 min–1), pseudo second order rate constant
	Isotherm	
Two-parameter model		
Freundlich	$q = K_F C_e 1^{/nF}$	C_e (mg/L), equilibrium concentration K_F [(mg/g) (L mg)$^{1/n}$], adsorption uptake constant nF, Freundlich parameter
Langmuir	$q = q_{max} K_L C / 1 + K_L C$	q_{max} (mg/g) maximum adsorption capacity of the adsorbent Ce (mg/L), equilibrium concentration K_L (L/mg) is the Langmuir constant

3.2.3 Characterization of MOFs after adsorption

1) Crystal structure by XRD

These data suggest that the ligands and metal nodes in these MOFs are able to endure the adsorption process without considerable degradation or structural collapse, as indicated by the XRD patterns for dry MOF samples obtained after adsorption.

As seen in Figure 9(a), the XRD pattern of UiO-66(Zr) upon adsorption is mostly unaltered, indicating that the adsorption process does not considerably modify the crystalline structure of UiO-66(Zr). The retention of peak locations and intensities suggests that adsorption proceeds without compromising the structural integrity of the framework. Nonetheless, these interactions don't appear to change the general structure, indicating that adsorption mostly takes place inside the pores and doesn't impact the MOF's backbone.

The strong zirconium-based nodes and solid ligand connections of UiO-66(Zr) probably contribute to its resistance to structural alterations during adsorption. For applications that call for repeated adsorption-desorption cycles, this stability is essential. Because of the strong Zr-O bonds and the protective function of the organic ligands, UiO-66(Zr) has intrinsic stability. The resistance of the framework against structural deformations during adsorption is attributed to both its stiffness and the spatial arrangement of its components.

Following adsorption, the MIL-100(Fe) XRD pattern exhibits modest variations in peak intensities from Figure 9(b), indicating small perturbations in the crystal structure that may be the result of interactions between the adsorbate and the iron centers or ligands. Nonetheless, it seems that the general crystallinity has been maintained.

MIL-100(Fe)'s crystalline structure was preserved upon adsorption, demonstrating the stability of its framework. According to this, adsorption does not substantially change the general structure of the MOF, which is consistent with the stability of MIL-100(Fe) under adsorptive stress. The minute variations in peak intensity may indicate interactions between the adsorbed molecules and the framework, which might modify the electron density or lead to small pore-level rearrangements. MIL-100(Fe)'s iron (III) clusters and organic ligands provide the framework a high level of chemical stability, allowing it to tolerate the addition of adsorbate molecules without suffering major structural changes. Certain MOFs, such as MIL-100(Fe), have a degree of flexibility that enables them to slightly modify their structural makeup to accommodate adsorbate molecules without sacrificing their overall crystallinity. As seen in Figure 9(c), the XRD pattern ZIF-8 following adsorption exhibits no discernible shift in peak positions or intensities, suggesting that the ZIF-8 framework is unaffected by adsorption and that its structural integrity is not jeopardized. This might suggest that the adsorbate and the Zn (II) ions or imidazolate linkers are interacting, which could have an impact on the pore environment or the overall crystallinity.

The strong structural integrity of ZIF-8 is demonstrated by the retention of peak locations after adsorption. For applications that need stability under changing environmental conditions or frequent cycles of adsorption and desorption, this resilience is essential. The minor variations in peak intensity may be an indication of how the adsorbate and ZIF-8 framework interact, perhaps influencing the Zn (II) nodes or imidazolate ligand orientation. Because these interactions are probably not harmful, ZIF-8 is able to keep its overall crystallinity. The preserved structure implies that, inside ZIF-8, adsorption takes place mostly in the pores, leaving the framework's backbone unaltered. This is in line with the anticipated behavior of MOFs with porous structures, such as ZIF-8, whose goal is to adsorb molecules while maintaining the material's integrity. The reason for ZIF-8's stability even after adsorption is multiple: Sturdy Metal-Ligand Connections: Strong Zn-N bonds in ZIF-8 provide a robust framework that is resistant to structural alterations brought on by interactions with the adsorbate. Pore Structure: Adsorbate molecules may be successfully accommodated by ZIF-8's pores due to their size and shape, which permits a substantial adsorption capacity without causing structural deformation.

Al-fum's XRD pattern following adsorption is substantially unaltered from Figure 9 (d), similar to UiO-66(Zr) and ZIF-8, indicating that the adsorption procedure does not negatively impact the MOF's crystalline structure. Al-fum may retain its porosity and structural integrity while interacting with adsorbates, as evidenced by the stability of its structure after adsorption. Al-fum is hence appropriate for uses like catalysis or gas storage that need for excellent adsorption process stability and efficiency.

To sum up, the examination of XRD patterns before to and during adsorption for these MOFs indicates that UiO-66(Zr), ZIF-8, and Al-fum retain their crystalline structures and integrity following adsorption, underscoring their resilience and appropriateness for a range of adsorption-related uses. MIL-100(Fe) exhibits minor alterations, suggesting a degree of interaction with adsorbates that modifies the framework somewhat but keeps it mostly intact. These findings suggest that these MOFs' ligands and metal nodes may endure the adsorption process without suffering from severe structural collapse or degradation.

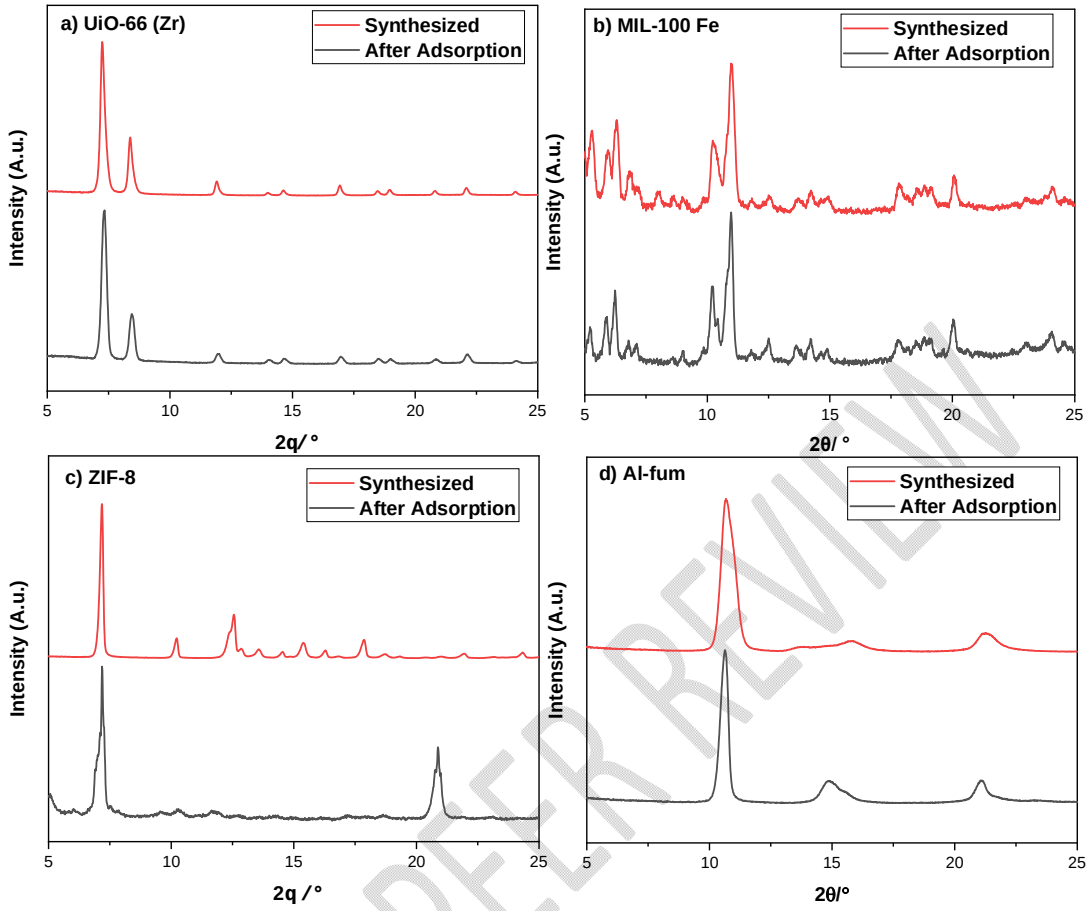

Figure 9. PXRD curves for a) UiO-66 (Zr), b) MIL-100 Fe, c) ZIF-8, d) Al-fum of synthesized and after adsorption MOFs

2) Chemical structure by FTIR

As seen in Figure 10(a), the carboxylate groups' peaks at 1583.8 cm^{-1} and 1507.7 cm^{-1} for UiO-66(Zr) after adsorption appear to have been slightly shifted or altered in intensity. This suggests that interactions between the adsorbate molecules and the carboxylate functionalities may have an impact on their electronic environment. The small shift of the 1392 cm^{-1} peak from the pre-adsorption spectra suggests that there may have been an alteration in the aromatic ring structures as a result of π-π interactions with the adsorbate. A significant shift from 1067.6 cm^{-1} to 1020.8 cm^{-1} may be due to variations in C-O stretching vibrations, indicating that ether or ester groups within the framework are impacted by adsorption. 677 cm^{-1}, 561.3 cm^{-1}, 473 cm^{-1} and 731.7 cm^{-1} The peaks' tiny shifts or intensities seen after adsorption imply that the framework's general integrity has been preserved, notwithstanding potential small modifications to the inorganic-organic interactions inside the MOF structure.

Variations in the peaks associated with aromatic rings and carboxylate groups indicate substantial interactions between adsorbate molecules and these functional groups, maybe through π-π interactions or hydrogen bonding. The adsorption behavior, electrical characteristics, and structure of the MOF are influenced by these interactions. Changes in the stretching vibrations of the C-O bond after adsorption suggest possible modifications in the ether or ester functionalities, which might affect the porosity or flexibility of the framework. The general structure of the MOF appears to have been maintained despite

these modifications, as shown by the constant metal-organic bending and stretching vibrations in the pre- and post-adsorption spectra.

As can be seen in Figure 10 (b), there is no O-H stretching peak for MIL-100(Fe) upon adsorption. The lack of this phenomenon after adsorption implies that the adsorbate has either displaced or interacted with water molecules or hydroxyl groups. The comparatively constant C-H stretching peaks at 2991 cm^{-1} and 2900 cm^{-1} show the durability of the framework's organic constituents after adsorption. The C=O stretching vibration shifts from 1634.5 cm^{-1} to 1632.5 cm^{-1}, indicating that the adsorbate and carboxylate groups may interact and change one other's electrical environments. Changes in the organic ligands' environment as a result of adsorption are reflected in the C-H bending and carboxylate stretching vibrations, which are 1450 cm^{-1} and 1382.9 cm^{-1}, respectively. The C-O stretching vibrations at around 1067.6 cm^{-1} suggest that the MOF structure interacts with ether or ester functions. The inorganic framework's integrity appears to be mostly preserved, with slight modifications perhaps indicating a tighter integration of the adsorbate inside the MOF structure, according to metal-oxygen vibrations (710.9 cm^{-1} and 631.7 cm^{-1}). The post-adsorption stability of C-H stretching vibrations demonstrates the robustness of the organic components in the framework. On the other hand, changes in the C=O stretching and C-H bending vibrations indicate possible interactions with adsorbate molecules, which might modify the carboxylate groups' electrical environment. Selectivity and capacity for various adsorbates can be affected by these interactions, which can affect the MOF's adsorption characteristics. Observed small variations in spectra, while preserving overall structural integrity, point to molecular-level modifications that might either increase or decrease the framework's usefulness for particular applications.

As seen in Figure 10 (c) of ZIF-8 upon adsorption, shifts in wide O-H and C-H stretching vibrations are suggestive of modifications to the organic linker environment and deposited water molecules. The stretching vibrations of C=N and C-N in imidazolate linkers exhibit peaks at 1571.6 cm^{-1} and 1422.5 cm^{-1}, respectively. These peaks indicate minor shifts or modifications in intensity that may indicate interactions between adsorbates and linkers, possibly changing their electrical environment. Peaks at 1310 cm^{-1} and 1179 cm^{-1} indicate changes in C-N stretching vibrations, which may indicate that adsorption has changed the electronic environment of imidazolate linkers. Changes in the C-N stretching or bending modes within the framework are reflected in a slight shift in the 1145.6 cm^{-1} peak. The framework's structural integrity is suggested by the peaks of 993.4 cm^{-1} and 759.1 cm^{-1}, with possible small modifications in the interactions between the metal and ligand. The stability of the Zn-N bond maxima at 689.1 cm^{-1-1} and 421.3 cm^{-1}, with very slight fluctuations, highlights the structural resistance to adsorptive stress.

Vibrational frequency changes of imidazolate linkers suggest possible changes in their electronic environment as a result of adsorption, which might impact the adsorption capabilities of the framework. The strong metal-organic bond strength that ensures framework stability is highlighted by slight changes in peaks related to Zn-N stretching vibrations post-adsorption. These interactions point to a combination of chemisorption and physisorption mechanisms occurring inside ZIF-8, wherein zinc ions and imidazolate linkers establish weak to moderate connections with adsorbate molecules.

The peak of 1611 cm^{-1} for Al-fum after adsorption, as seen in Figure 10 (d), marginally displaced from 1619.3 cm^{-1} before to adsorption, indicating a little modification in the carboxylate groups, maybe as a result of interactions with the adsorbate molecules. This little shift, from 1424.2 cm^{-1} pre-adsorption to 1422.5 cm^{-1} post-adsorption, may be the result of modifications to the structures of the aromatic rings or their interactions with the molecules of the adsorbate. 1154.7 cm^{-1}, 987.3 cm^{-1}, 804.7 cm^{-1}, and 719.5 cm^{-1}: These bands indicate modifications in the functionalities of the ether, ester, or alcohol following adsorption and are compatible with changes in C-O stretching and bending vibrations. 689.1 $cm^{-1}$and 649.5 cm^{-1}: The persistence of these peaks indicates that the integrity of the inorganic framework is

mainly preserved, with small variations perhaps indicating a closer integration of the adsorbate inside the MOF structure.

The adsorption-induced rearrangement of water molecules and hydroxyl groups within the MOF is shown by the shift in O-H stretching vibrations. The interaction of adsorbate molecules with carboxylate groups, either through hydrogen bonding or coordination to metal sites, is shown by the change in C=O stretching vibrations. The little change in C=C stretching vibrations indicates that π-π interactions have an impact on aromatic components, which in turn influences structural dynamics. Adsorption's effect on functional groups is shown by changes in C-O stretching vibrations.

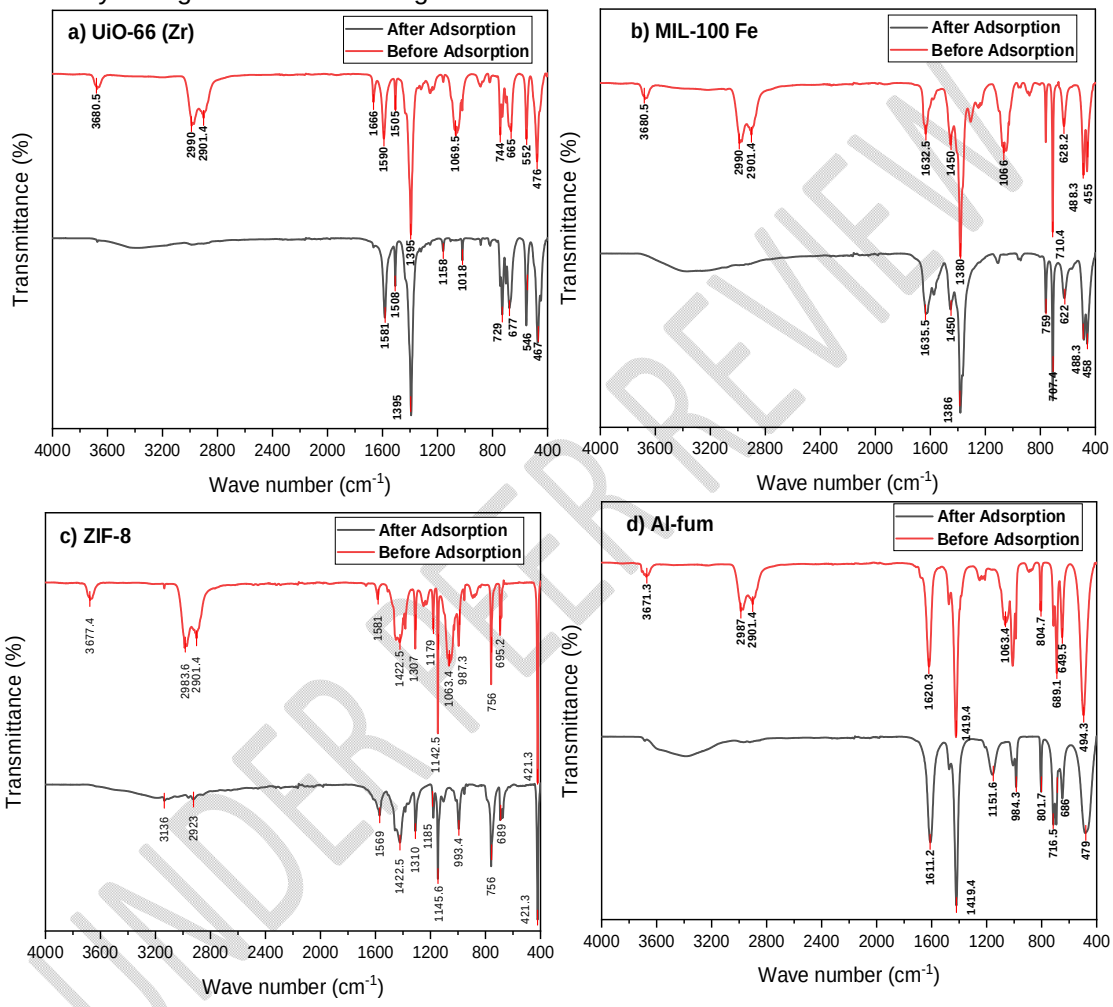

Figure 10. FT-IR spectra of (a) UiO-66(Zr), (b) MIL-100(Fe), (c) ZIF-8, (d) Al-fum after adsorption

3) Morphology by SEM

From Figure 11(a), the individual octahedral crystals of UiO-66(Zr) are more clearly evident. Every crystal surface has a rougher roughness that suggests potential adsorption sites or surface changes; in contrast, pure states often show smoother textures. For both states, UiO-66(Zr) MOF are usually octahedral or cubic in form.

As seen in Figure 11(b), MIL-100(Fe) in the post-adsorption condition retains its polyhedral crystal form without undergoing any appreciable morphological alterations. The consistency of the crystal size and the retention of the surface shape after adsorption imply that the MOF's structural integrity is not negatively impacted by the adsorption process. Surface

irregularities and sporadic clumps may be signs of interactions with adsorbed molecules, However, over the range of observed magnifications, the MIL-100(Fe) appears to exhibit good stability and preservation of its crystalline structure upon adsorption.

ZIF-8's spherical shape is still discernible from Figure 11(c) upon adsorption. There is little evidence of substantial morphological changes or collapse of individual particles, and the surface roughness is suggestive of adsorption processes. In comparison to its pristine form, the surface exhibits increased granularity, suggesting the presence of adsorbed species. The finer features of the surface textures are more noticeable, but the particle size appears to be constant.

Ultimately, the roughened surfaces and perhaps small agglomerations in the SEM picture provide strong proof that adsorption has occurred. However, ZIF-8's strong framework is essentially unchanged, which is a favorable feature for sorption applications where material stability is essential.

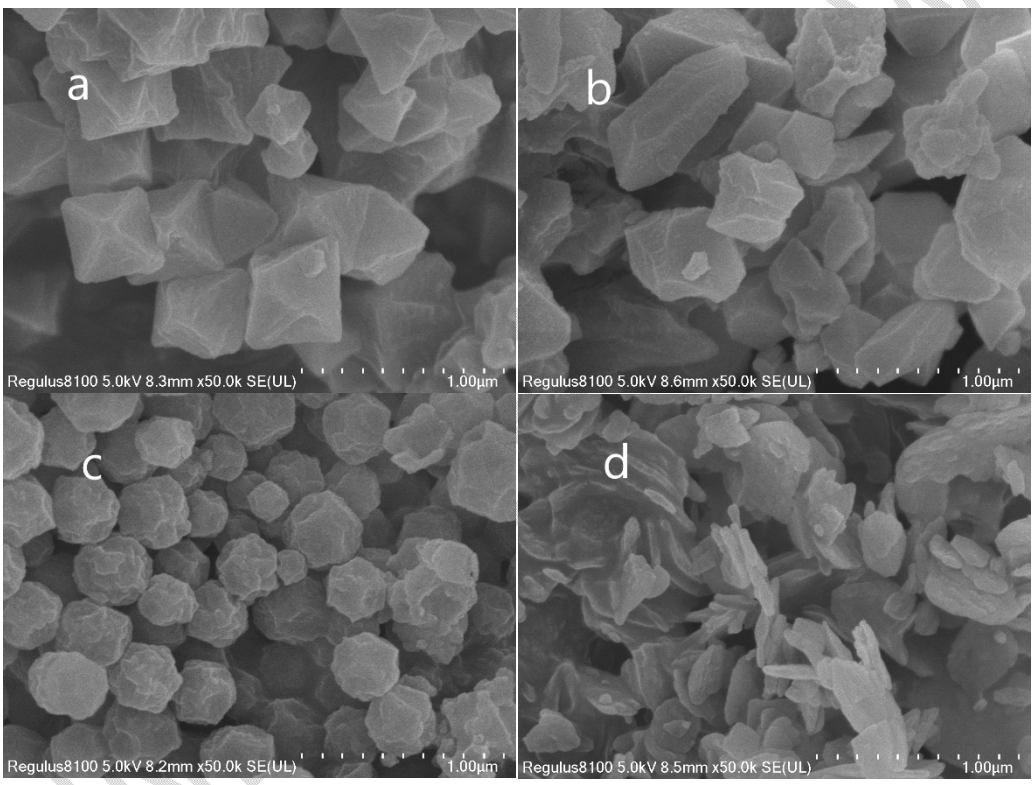

Figure 11. SEM images of a) UiO-66(Zr), b) MIL-100(Fe), c) ZIF-8, d) Al-fum after adsorption

As seen in Figure 11(d), the Al-fum particles exhibit elongated characteristics in their post-adsorption condition, which may be related to the adsorption process. The uneven, rougher, and less defined margins of the morphology imply that the adsorption may cause changes in the form of the particles or encourage aggregation. Particles vary in size, but they fall between sub-micrometer to micrometer. There is a mixture of more spherical and flakes-like particles.

4 conclusions and recommendations

4.1 conclusions

In this work, the potential of metal-organic frameworks (MOFs) for water purification is thoroughly investigated, with a focus on the removal of humic acid (HA) from aquatic

systems. Humic substances, such as HA, are well-known for their detrimental effects on water quality, which include changing the water's aesthetic appeal and potability and promoting the growth of harmful algal blooms. While somewhat effective, traditional water treatment methodologies are not up to the challenges presented by these contaminants, thereby requiring more sophisticated and effective treatment technologies. Our research addressed this need by synthesizing and using four different MOFs (UiO-66 (Zr), MIL-100 (Fe), ZIF-8, and Al-fumarate (Al-fum)) and evaluating their potential for adsorption processes in water treatment. The comparison study investigated the ideal pH for HA removal, the ideal adsorption capacity, and the equilibrium time for every MOF.

- UiO-66 (Zr) was examined for its fast equilibrium time of less than 15 minutes, its adsorption capacity of 55 mg/g, and its ability to increase the MOF in acidic conditions. These results were obtained after the compound was successfully synthesized, as demonstrated by the matching of synthesized and simulated peaks, and its microporous structure, as demonstrated by N2 sorption and porous properties. This important discovery shows the MOFs' catalytic potential in sedimentation and the ensuing removal of pollutants.
- With the greatest surface area and pore volume of 1820m2/g and 0.81cm3/g, respectively, ZIF-8 emerged as the front-runner among all MOFs after being successfully synthesized. It is particularly noteworthy for its extraordinary adsorption capacity of 754 mg/g, which can be due to its strong base interaction with HA. Since both HA and ZIF-8 are basic, this MOF exhibited excellent HA removal at a neutral pH of 7, indicating a stronger interaction than with previous MOFs. Considering its simple room-temperature synthesis and effectiveness compared to other MOFs like UiO-66 (Zr) and MIL-100 (Fe), which need more energy-intensive solvothermal techniques, ZIF-8 is a promising option for HA remediation.
- MIL-100 (Fe), which came after ZIF-8, had the greatest surface area of 1600 m2/g and the largest pore volume of 0.56 cm3/g. It also investigated the mesoporous structure, which is better suited for larger molecules, and it looked at a quick equilibrium time and a good adsorption capacity of 129 mg/g, which makes it preferable in acidic conditions.
- Al-fumarate (Al-fum), which may be preferred in both acidic and basic environments, reached mesoporous structure as demonstrated by the N2 sorption test, had the slowest equilibrium time among the studied MOFs, and an amazing adsorption capacity of 215 mg/g after ZIF-8. The Al-fum results support taking these operational factors into account when using MOFs to actual water purification problems.

In order to understand the processes of interaction between MOFs and HA as well as the structural and functional integrity of MOFs after treatment, characterization analyses were carried out. UiO-66 (Zr) and Al-fum showed no structural changes during X-ray diffraction (XRD) post-adsorption, but MIL-100 Fe and ZIF-8 showed minimal structural modifications as a result of the HA interaction. The results of Fourier-transform infrared spectroscopy (FTIR) suggested that MOFs and HA interacted; in particular, the loss of peaks in the 2800–3800 cm-1 region suggested that functional groups may have been involved. These results were further supported by scanning electron microscopy (SEM) investigations, which showed that the MOF shape remained constant after adsorption, maintaining the microscale structural integrity.

Our thorough investigation concludes by highlighting MOFs' revolutionary potential as a cutting-edge method of water filtration. ZIF-8 is notable for its effectiveness and useful synthesis; nonetheless, every MOF has distinct qualities that may be customized to meet certain therapeutic requirements.

The adsorption capacities of the synthesized MOFs, including UiO-66(Zr), MIL-100(Fe), ZIF-8, and Al-fum, demonstrate significant potential when compared to commonly used adsorbents like activated carbon. Preliminary results indicate that these MOFs offer competitive or even superior performance in terms of humic acid removal. This is attributed to their high surface area, well-defined porosity, and functional groups tailored for specific

interactions with humic acid molecules. Further comparative studies are necessary to quantify the exact adsorption capacities relative to activated carbon and other advanced materials to confirm these findings comprehensively[4].

While the current study focuses on the adsorption of humic acid in controlled laboratory conditions, future research will include testing the performance of these MOFs in real-world water samples. The presence of other contaminants, such as heavy metals, organic pollutants, and competing ions, could impact the adsorption efficiency of the MOFs. These substances may compete for active sites on the MOFs or alter the chemical environment, potentially reducing their effectiveness. Evaluating MOF performance in complex water matrices will provide a more accurate assessment of their practical applicability in real-world scenarios.

The regeneration and reusability of the MOFs are critical factors in determining their overall effectiveness and economic viability. Preliminary studies suggest that the synthesized MOFs can be regenerated through processes such as solvent washing, thermal treatment, or chemical regeneration. The ability to maintain high adsorption capacity after multiple regeneration cycles will significantly enhance the economic feasibility of using MOFs for humic acid removal. Ongoing research aims to optimize regeneration protocols to ensure minimal loss of adsorption efficiency and structural integrity over repeated use.

4.2 Recommendations

To encourage the use of metal-organic frameworks (MOFs) in water purification procedures, the following suggestion can be made:

1) Additional Study on MOF Variants Further research into MOFs that can be manufactured via less energy-intensive techniques and offer high efficiency in pollutant removal should be encouraged, given the success of ZIF-8, which may be attributed to its room-temperature synthesis and high adsorption capacity
2) Development of Hybrid Systems: To reach complete water treatment solutions, look into the development of hybrid systems that integrate MOFs with other treatment technologies, such membrane filtration, advanced oxidation process
3) Considering including additional experiments to test the stability of the MOFs in different water chemistries (e.g., varying ionic strengths, presence of competing ions) to better simulate real-world conditions, include a brief economic analysis comparing the cost-effectiveness of using MOFs for humic acid removal versus other traditional water treatment methods. This could provide valuable insights for practical implementation.
4) Investigating and reporting on the long-term performance and durability of the MOFs under continuous operation conditions. This information would be crucial for understanding their practical applicability in water treatment facilities.

COMPETING INTERESTS

Authors have declared that they have no known competing financial interests OR non-financial interests OR personal relationships that could have appeared to influence the work reported in this paper.

Disclaimer (Artificial intelligence)

Author(s) hereby declare that NO generative AI technologies such as Large Language Models (ChatGPT, COPILOT, etc) and text-to-image generators have been used during writing or editing of manuscripts.

References

[1] Eikebrokk B, Vogt R D, Liltved H. NOM increase in Northern European source waters: discussion of possible causes and impacts on coagulation/contact filtration processes [J]. Water Supply, 2004, 4(4): 47-54.

[2] Sillanpää M. Natural organic matter in water: Characterization and treatment methods [M]. Butterworth-Heinemann, 2014.

[3] Sillanpää M, Ncibi M C, Matilainen A. Advanced oxidation processes for the removal of natural organic matter from drinking water sources: A comprehensive review [J]. Journal of environmental management, 2018, 208: 56-76.

[4] Kaur H, Devi N, Siwal S S, et al. Metal–Organic Framework-Based Materials for Wastewater Treatment: Superior Adsorbent Materials for the Removal of Hazardous Pollutants [J]. ACS Omega, 2023, 8(10): 9004-9030.

[5] Li B, Wen H M, Cui Y, et al. Emerging Multifunctional Metal-Organic Framework Materials [J]. Adv Mater, 2016, 28(40): 8819-8860.

[6] Rowsell J L C, Yaghi O M. Metal–organic frameworks: a new class of porous materials [J]. Microporous and Mesoporous Materials, 2004, 73(1): 3-14.

[7] Furukawa H, Cordova K E, O'keeffe M, et al. The Chemistry and Applications of Metal-Organic Frameworks [J]. Science, 2013, 341(6149): 1230444.

[8] Liu X, Shan Y, Zhang S, et al. Application of metal organic framework in wastewater treatment [J]. Green Energy & Environment, 2022.

[9] Yaghi O M. Crystalline metal-organic microporous materials [Z]. Google Patents. 1997

[10] Tchinsa A, Hossain M F, Wang T, et al. Removal of organic pollutants from aqueous solution using metal organic frameworks (MOFs)-based adsorbents: A review [J]. Chemosphere, 2021, 284: 131393.

[11] Karimi M, Mehrabadi Z, Farsadrooh M, et al. Chapter 4 - Metal–organic framework [M]//GHAEDI M. Interface Science and Technology. Elsevier. 2021: 279-387.

[12] Zhu X, Li B, Yang J, et al. Effective adsorption and enhanced removal of organophosphorus pesticides from aqueous solution by Zr-based MOFs of UiO-67 [J]. ACS applied materials & interfaces, 2015, 7(1): 223-231.

[13] Zhu Z, Jiang Y, Wang Z, et al. Effective removal of humic acid by mesoporous Zr-MOF adjusted through SDBS [J]. Environ Sci Pollut Res Int, 2022, 29(48): 73043-73051.

[14] Tambat S N, Sane P K, Suresh S, et al. Hydrothermal synthesis of NH2-UiO-66 and its application for adsorptive removal of dye [J]. Advanced Powder Technology, 2018, 29(11): 2626-2632.

[15] Nehra M, Dilbaghi N, Singhal N K, et al. Metal organic frameworks MIL-100(Fe) as an efficient adsorptive material for phosphate management [J]. Environmental Research, 2019, 169: 229-236.

[16] Yang J-C, Yin X-B. CoFe2O4@MIL-100(Fe) hybrid magnetic nanoparticles exhibit fast and selective adsorption of arsenic with high adsorption capacity [J]. Scientific Reports, 2017, 7(1): 40955.

[17] Yang J C, Yin X B. CoFe(2)O(4)@MIL-100(Fe) hybrid magnetic nanoparticles exhibit fast and selective adsorption of arsenic with high adsorption capacity [J]. Sci Rep, 2017, 7: 40955.
[18] Liu D, Wu Y, Xia Q, et al. Experimental and molecular simulation studies of CO 2 adsorption on zeolitic imidazolate frameworks: ZIF-8 and amine-modified ZIF-8 [J]. Adsorption, 2013, 19: 25-37.
[19] Lin K-Y A, Chang H-A. Efficient Adsorptive Removal of Humic Acid from Water Using Zeolitic Imidazole Framework-8 (ZIF-8) [J]. Water, Air, & Soil Pollution, 2015, 226(2): 10.
[20] Ke F, Peng C, Zhang T, et al. Fumarate-based metal-organic frameworks as a new platform for highly selective removal of fluoride from brick tea [J]. Scientific Reports, 2018, 8(1): 939.
[21] Zhao X, Wang T, Du G, et al. Effective Removal of Humic Acid from Aqueous Solution in an Al-Based Metal–Organic Framework [J]. Journal of Chemical & Engineering Data, 2019, 64(8): 3624-3631.
[22] Furukawa H, Gándara F, Zhang Y-B, et al. Water Adsorption in Porous Metal–Organic Frameworks and Related Materials [J]. Journal of the American Chemical Society, 2014, 136(11): 4369-4381.
[23] Chen L, Wang X, Rao Z, et al. One-pot Synthesis of the MIL-100 (Fe) MOF/MOX Homojunctions with Tunable Hierarchical Pores for the Photocatalytic Removal of BTXS [J]. Applied Catalysis B: Environmental, 2022, 303: 120885.
[24] Jian M, Liu B, Liu R, et al. Water-based synthesis of zeolitic imidazolate framework-8 with high morphology level at room temperature [J]. RSC Advances, 2015, 5: 48433-48441.
[25] Teo H W B, Chakraborty A, Kayal S. Formic acid modulated (fam) aluminium fumarate MOF for improved isotherms and kinetics with water adsorption: Cooling/heat pump applications [J]. Microporous and Mesoporous Materials, 2018, 272: 109-116.
[26] Naseem S, Aslam H M, Abbas A, et al. Synthesis and Application of Cobalt-based Metal-organic Framework for Adsorption of Humic Acid from Water [J]. Chemical and Biochemical Engineering Quarterly, 2022, 36.
[27] Qian J, Sun F, Qin L. Hydrothermal synthesis of zeolitic imidazolate framework-67 (ZIF-67) nanocrystals [J]. Materials Letters, 2012, 82: 220-223.
[28] Thakkar H, Eastman S, Al-Naddaf Q, et al. 3D-Printed Metal-Organic Framework Monoliths for Gas Adsorption Processes [J]. ACS Appl Mater Interfaces, 2017, 9(41): 35908-35916.
[29] Winarta J, Shan B, Mcintyre S M, et al. A Decade of UiO-66 Research: A Historic Review of Dynamic Structure, Synthesis Mechanisms, and Characterization Techniques of an Archetypal Metal–Organic Framework [J]. Crystal Growth & Design, 2020, 20(2): 1347-1362.
[30] Chen M L, Zhou S Y, Xu Z, et al. Metal-Organic Frameworks of MIL-100(Fe, Cr) and MIL-101(Cr) for Aromatic Amines Adsorption from Aqueous Solutions [J]. Molecules, 2019, 24(20).
[31] Hurlock M J, Christian M S, Rimsza J M, et al. Design Principles Guiding Solvent Size Selection in ZIF-Based Type 3 Porous Liquids for Permanent Porosity [J]. ACS Mater Au, 2024, 4(2): 224-237.

[32] Karmakar S, Dechnik J, Janiak C, et al. Aluminium fumarate metal-organic framework: A super adsorbent for fluoride from water [J]. Journal of Hazardous Materials, 2016, 303: 10-20.

33Alomar T, Qiblawey H, Almomani F, Al-Raoush RI, Han DS, Ahmad NM. Recent advances on humic acid removal from wastewater using adsorption process. Journal of Water Process Engineering. 2023 Jul 1;53:103679.

34 Zhao N, Ju F, Pan H, Tang Z, Ling H. Molecular dynamics simulation of the interaction of water
and humic acid in the adsorption of polycyclic aromatic hydrocarbons. Environmental Science and Pollution Research. 2020 Jul;27:25754-65.